VAMAS

Technical Working Area 3

Ceramics

CEN/VAMAS PHASE VOLUME FRACTION ROUND ROBIN

FINAL TECHNICAL REPORT

by

M Hendrix, E G Bennett, R Morrell, L J M G Dortmans, G de With

May 1998

VAMAS Technical Report No. 35

ISSN 1016 - 2186

Versailles Project on Advanced Materials and Standards
Canada, EC, Germany, France, Italy, Japan, UK, USA

VAMAS Technical Report No 35.

CEN/VAMAS Phase Volume Fraction Round Robin

by

M. Hendrix[1], E. Bennett[2], R. Morrell[2], L.J.M.G. Dortmans[3] and G. de With[1]

[1] *Eindhoven University of Technology, CTK-TUE-TVM, P.O. Box 513, 5600 MB Eindhoven, The Netherlands.*

[2] *National Physical Laboratory, Teddington, Middlesex, United Kingdom TW11 0LW.*

[3] *Institute of Applied Physics, CTK-TNO, P.O. Box 595, 5600 AN Eindhoven, The Netherlands.*

Abstract

This report describes the analysis of the results of a round robin conducted under the auspices of CEN Technical Committee 184, Advanced Technical Ceramics. The objective was to evaluate the potential accuracy and repeatability of making manual or automatic image analysis characterisations of phase volume fraction in multiphase ceramic materials. Participants were provided with a series of micrographs, including one generated by computer, and a ceramic sample, of the same material used for some of the supplied micrographs, from which a further micrograph had to be prepared by the participant using his/her own methods. The micrographs were analysed manually using a grid intersection counting method, and automatically using a grey level pixel counting method. It has been found that the conditions employed for the manual measurements gave acceptable and explainable scatter of results, and provided a suitable basis for preparation of a CEN standard. In contrast, the results obtained using AIA were less reliable and more widely scattered owing to factors involved in inputting the image (re-formatting, re-sizing, or analysis of part areas only) and the difficulties of assigning features to the count for particular phases due to the contrast variations across these phases.

ISSN 1016 - 2186

NOTE: This report has been approved by CEN TC184 by resolution at its meeting of 12 May 1998 for unlimited distribution.

Approved on behalf of Managing Director, NPL, by Dr D Eastham, Commercial Manager, Centre for Materials Measurement and Technology.

Signature: .....
Commercial Manager

Date: .....

Signature: .....
Principal Author

Date: .....

Contents

List of participants

E. Bennett	National Physical Laboratory	United Kingdom
V. Biasini / F. Monteverde	Research Institute for Ceramic Technology	Italy
I. Bowcock	British Acrospace Airbus Limited	England
K. M. Broek / M. Roos	ECN	The Netherlands
D. Delfosse / U. Güdel	EMPA	Switserland
J. Dusza / B. Balloková / T. Murajda	Institute of Materials Research of SAS	Slovakia
J. Hahn	Korea Research Institute of Standards and Science	South Korea
M. Hendrix	Eindhoven University of Technology	The Netherlands
M. Labanti / G. Martignani	ENEA CRNM INN-NUMA-IMAP	Italy
M. Mizuno / J.W. Cao	Japan Fine Ceramics Centre	Japan
P. Moretto / J. Casado	Joint Research Centre - IAM	The Netherlands
U. Mücke	BAM, Federal Institute for Materials Research and Testing	Germany
G. Quinn / H. Maupas	NIST, Ceramic Division	USA
M. Reece	Department of Materials Queen Mary And Westfield College	United Kingdom
J. Rheinländer / P.V. Jensen	RISO National Laboratory	Denmark
A. Robinson / A. Griffiths	British Nuclear Fuels PLC	United Kingdom
S. Sakaguchi	National Industrial Research institute of Nagoya	Japan
C. Schmid / A. Rossi	University of Trieste	Italy
S. Seifert	RBB R&D	England
R.W. Stannard / J. Penn	Morgan Materials Technology LTD.	England
H. Tanaka	National Institute for Research Inorganic Materials	Japan
R. Teti / F. Parretta	University of Naples "Frederico II"	Italy
A. Tucci	Italian Ceramic Centre	Italy
W. Vandermeulen / R. Kemps	VITO	Belgium
J. R. Varner	NYS College of Ceramics Alfred University	USA
R.N. White	Ceram Research	United Kingdom
G. Zies / B. Fenk	Staatliche Materialprüfungsanstalt MPA	Germany

1. Introduction

The characterisation of microstructures in materials, such as advanced technical ceramics, requires test procedures in which the experimental design minimises the risk of errors from all sources. The CEN Technical Committee 184, Working Group 3, expressed the need for a standard procedure for determining phase volume fraction and/or porosity from micro-sections of materials. In order to provide evidence of the suitability of a manual technique for formal standardisation, a round robin was instituted. This was a follow-up to an earlier successful CEN/VAMAS round robin [1] in which the measurement of mean linear grain size was examined. The stereological principles of the volume fraction measurements are well-known [2,3]. Amongst other things, the preparation of the test-piece, the selected area of the microstructure and the techniques for assessing microstructural parameters, may influence all the results of the subsequent analysis. As for the earlier round robin, this present study should reveal these influences. Furthermore, the results would give an indication of the reliability and reproducibility relevant to these kinds of measurements for intended users, such as research or control laboratories, and would provide endorsement of a new standard.

This report gives an overview of the results of the round robin run by CEN TC184/WG3 and extended to VAMAS nations. Twenty-seven participants from Europe, USA and Asia took part.

2. Objectives

This round robin is designed to reveal the scatter which occurs in the determination of the volume fraction of phases and/or porosity in multiphase advanced technical ceramics, and thus to provide a possible confidence level that can be used in citation of results. It can furthermore be used to determine the reliability and reproducibility of the results using materials of increasing complexity. This could lead to an ability to correlate the attained scatter of the results with the conditions of measurement.

3. Methods and Materials

In the round robin, both manual and automatic image analysis (AIA) methods could be used to determine the phase volume fraction and/or porosity.

Manual image analysis is achieved by placing a grid over an image of the microstructure. The analysis deals with counting the number of intersections of the grid lying over each phase, designated as 'point counting'. Normalising this number of intersections for each phase by the total number of intersections will give the respective volume fractions. Intersections lying on phase boundaries are counted half for each phase. The grid used for the measurements had a true grid size of 8 mm, Figure 3.1. The choice of this grid size is explained in Section 4.1. Subjective decisions have to be made as to positioning of the grid relative to the microstructure, the position of the grid intersection relative to the phase boundaries, and the true position of these phase boundaries within the resolution of their delineation by etching or phase contrast.

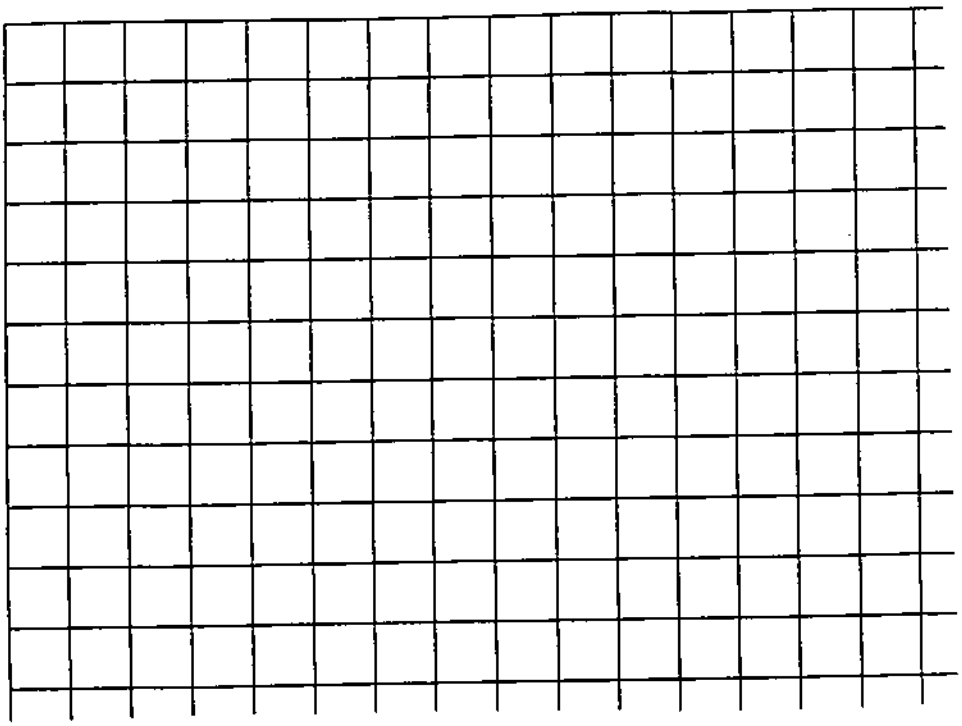

Figure 3.1 Portion of the grid used for the manual analysis.

Automatic image analysis deals typically with counting pixels of different grey levels in a digitised image, designated as 'pixel counting'. The digitised interpretation of the image leads to a spread of grey levels which have to be correctly partitioned between the different phases. If the image analysis software can define a grid of points, the manual method can be simulated. In the round robin, six micrographs were used for both manual and automatic image analysis with differing degrees of difficulty of interpretation.

Part 1 of this round robin was composed of the analysis of five micrographs prepared by the organizers. The supplied micrographs consisted of:

A. A computer generated 'ideal' microstructure with a clear delineation of grain boundaries and grey/white contrast between the phases without porosity, Figure 3.2.

The area ratio of the two phases is about 1 (Table 3.1), consisting of about 200 grains each. The expected scatter, using the point counting method, is likely to be caused by the positioning of the grid. Due to the clear contrast between the phases, one might expect no difficulties in relation to the differentiation of the phases. Therefore, the scatter on the results, describing the whole micrograph, can be denoted as being the minimum attainable scatter inherent in this method and set-up[1]. This is also valid for

[1] The scatter is dependent on the volume fractions of the phases present in the micrograph. If the volume fraction of one of the phases increases, the statistics of this phase improve due to the increase in number of intercepts or the number of pixels. However, the statistics of the other phase(s) worsen, and thereby the potential fractional scatter increases. Therefore, the description of the micrograph or microstructure, is related to all the phases, and its correctness is determined by the phase with the largest scatter. In addition, lack of perfect homogeneity of microstructure leads to increased unreliability of a single result relative to the true average for the material. This round robin used single micrographs to reduce the effort involved, but this is not normal recommended practice, which is to select at least three areas of the same material.

the pixel counting method. Furthermore, the scatter might be dependent on the maximum resolution of the automatic image analyser employed.

Table 3.1 - The "true" analysis of the computer-generated microstructure

'Phase'	Actual number of pixels in 1883 x 1883 image	'Phase' volume fraction, %	Normalised 'phase' volume fraction ignoring boundaries, %
Dark phase	1,632,696	46.05	49.92
Light phase	1,627,092	45.89	50.08
Boundary area	285,901	8.06	-
Total pixel count	3,545,689	100.00	100.00

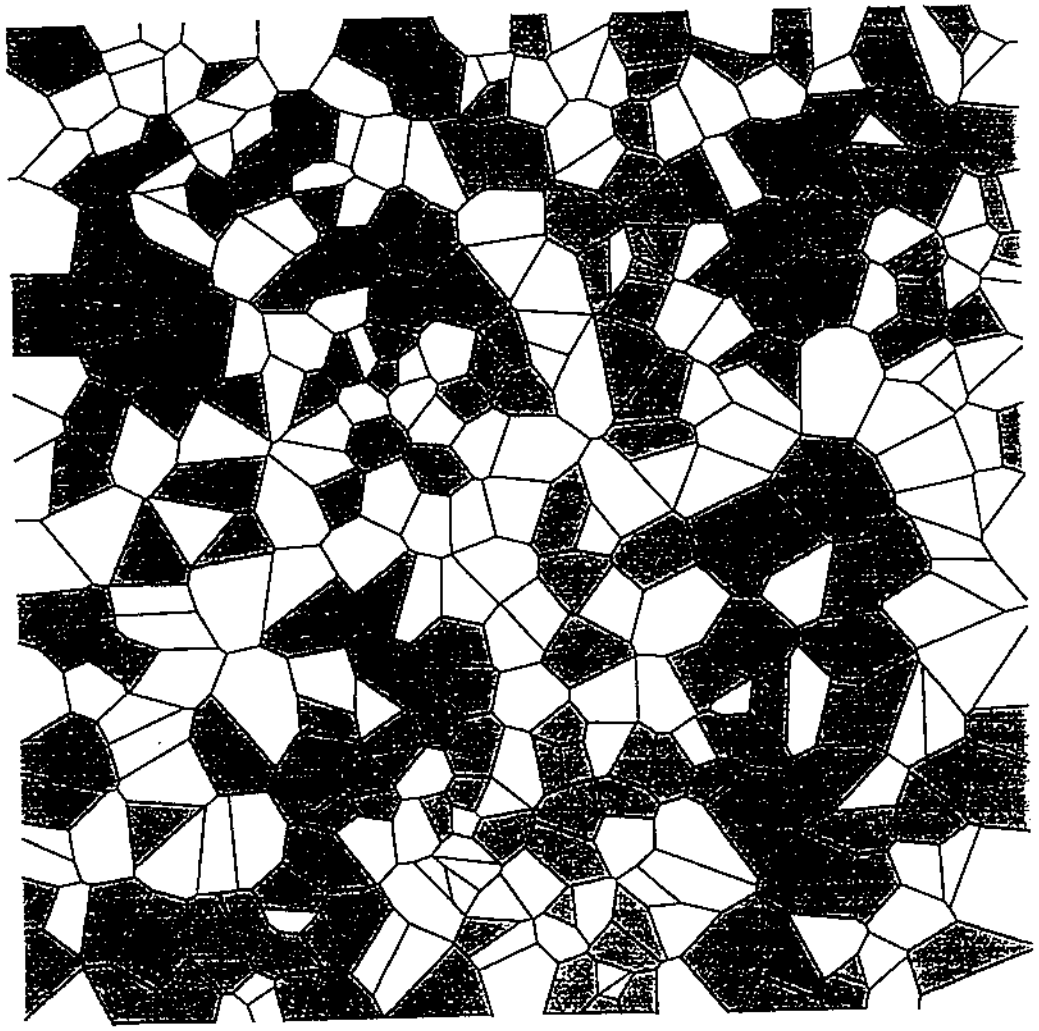

Figure 3.2 Micrograph A, a Dirichlet tessellation of two-phase 'microstructure' with finite width grain boundaries.

B. A secondary electron image of a two-phase barium titanate type ceramic showing a light grey barium titanate phase, a dark grey titanium dioxide phase, and a black phase which is porosity, Figure 3.3.

The area ratio of the two ceramic phases is similar to that of the computer tessellation micrograph. One might expect, however, some difficulties connected with the differentiation of the phases as a result of contrast variations across each grain. Therefore, using the point counting method, the deviation in the results from the participants might not only caused by the position of the grid but also by the misinterpretation of the phases and the presence of some pores. The scatter for the pixel counting method will be mainly dependent on the problem of partitioning of the grey values of the different phases.

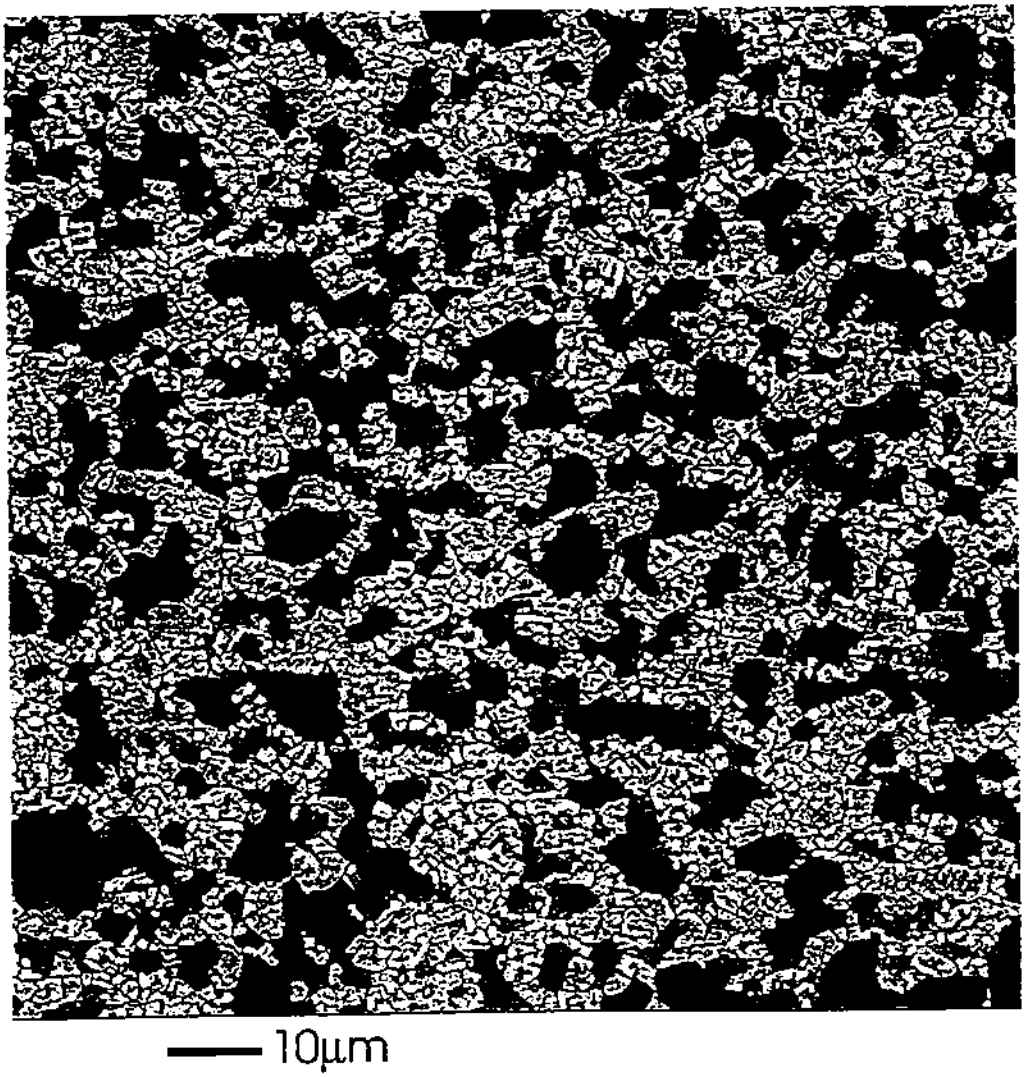

Figure 3.3 Micrograph B, a two-phase barium titanate material with minimal porosity.

C. A backscattered electron image of an alumina/zirconia ceramic which clearly delineates the zirconia phase and minimises the contrast from other features such as thermally etched grain boundaries and shallow pores, Figure 3.4.

The area fraction of the zirconia phase, the light-coloured phase in SEM images, is less than 10%. The scatter of results between participants can be caused by the positioning of the grid, the misinterpretation of the phases, the presence of some pores, the small amount of zirconia phase and the partitioning of the grey values, exacerbated by the relatively noisy image produced by this technique.

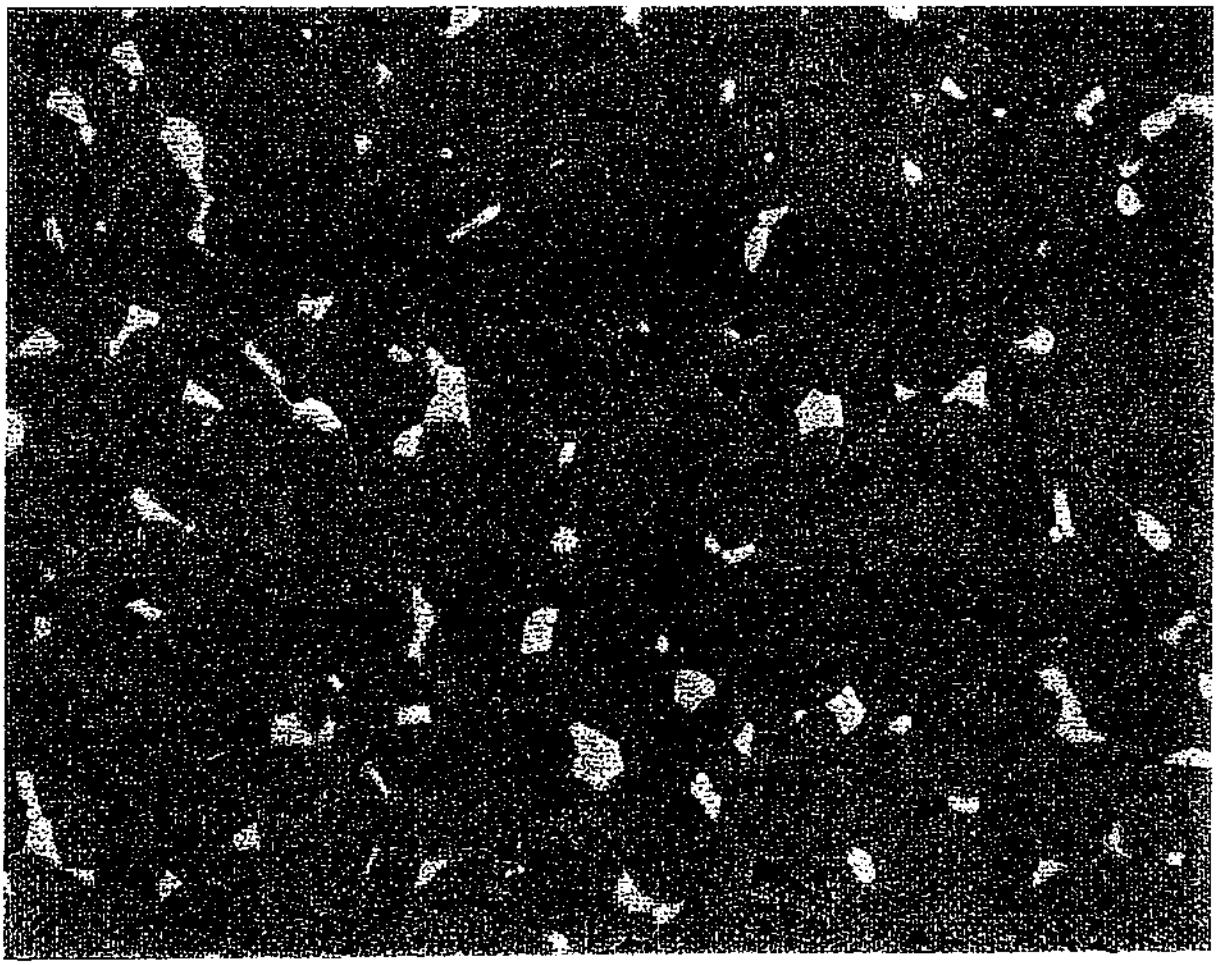

Figure 3.4 Micrograph C, a backscattered scanning electron micrograph of an alumina zirconia material produced by capturing five repeats with frame averaging over 20 scans to reduce noise.

D. A secondary electron image of the same area as micrograph C, but having additional contrast on the edges of the pores and the grain boundaries, Figure 3.5.

Micrograph C could be used as an aid for the interpretation of this micrograph. The scatter of the results might be expected to be less than that of micrograph C, primarily because of lower noise and better resolution.

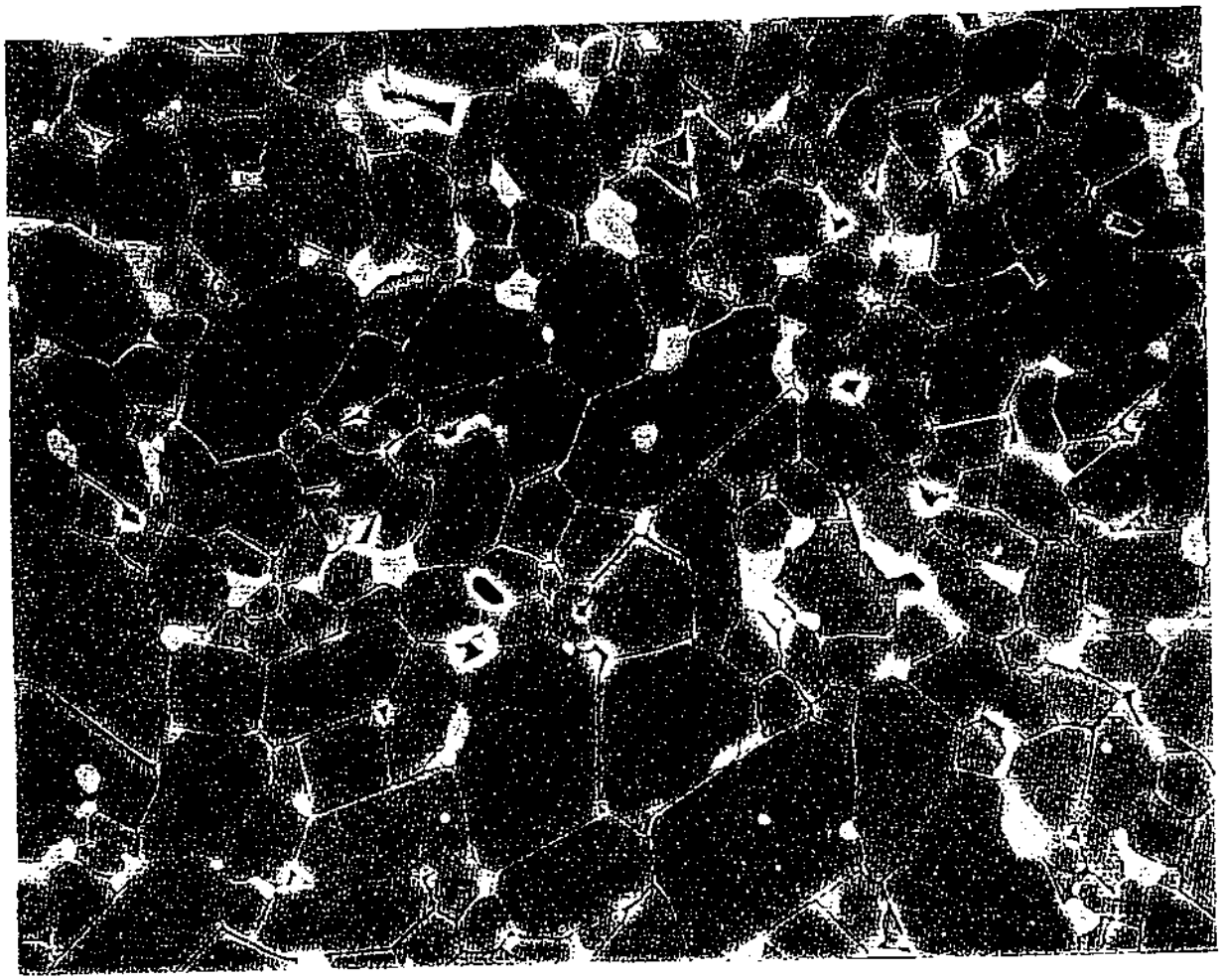

Figure 3.5 Micrograph D, as Micrograph C but a secondary electron image of the same area with enhanced contrast at pore edges and visible topography. Micrograph C could be used to support the identification of features in Micrograph D.

E A secondary electron image of a different area from the same specimen used in part C and D, Figure 3.6. However, in this case there is no accompanying backscattered image to aid interpretation by the participant.

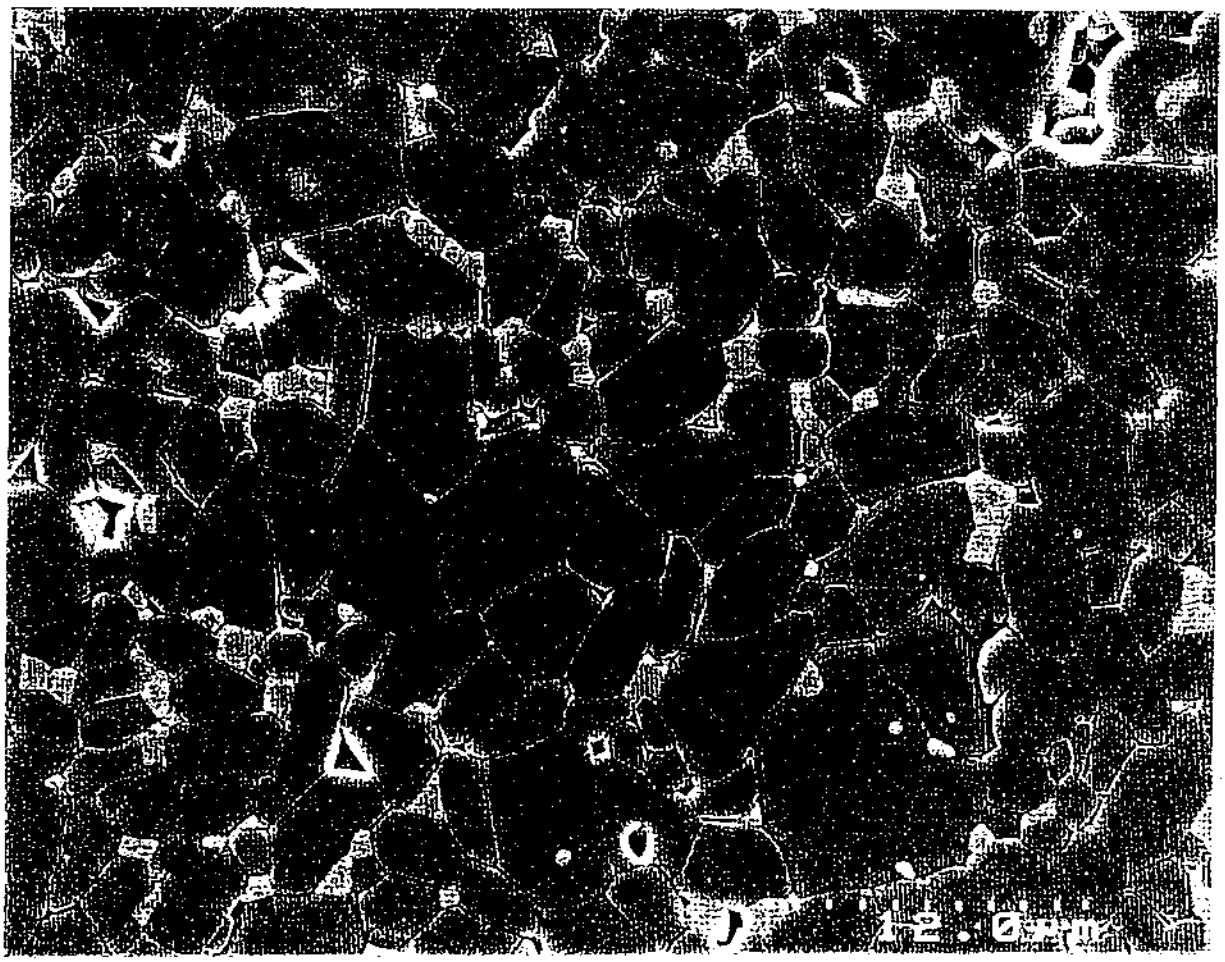

Figure 3.6 Micrograph E, as Micrograph D but a different area of the same test piece, and with no supporting backscattered image.

These images were supplied as paper copies (glossy photo prints, 18x23 cm) and in digitised form as compressed .TIF files on floppy disks. For the manual method, the paper copies were to be used, while for AIA, in order to adapt to the range of systems and facilities available to the participants, the images could be re-photographed via video systems or scanners, or loaded directly as the digitised files which were in executable form and self-expanding.

Part 2 of the round robin dealt not only with the analysis of a micrograph but also with the preparation by the participants of an alumina/zirconia ceramic sample, as also used for micrographs C, D and E. The preparation involved at least grinding and polishing. Etching of the sample was considered not to be essential. For the participant, the presence of some grain tear-out may influence the results, and certainly complicates the decision on what is a genuine pore. A nominal temperature of 1450 °C and a duration of 15 min is probably sufficient if thermal etching is employed to delineate grain boundaries. Figure 3.7 shows a micrograph from one of the participants.

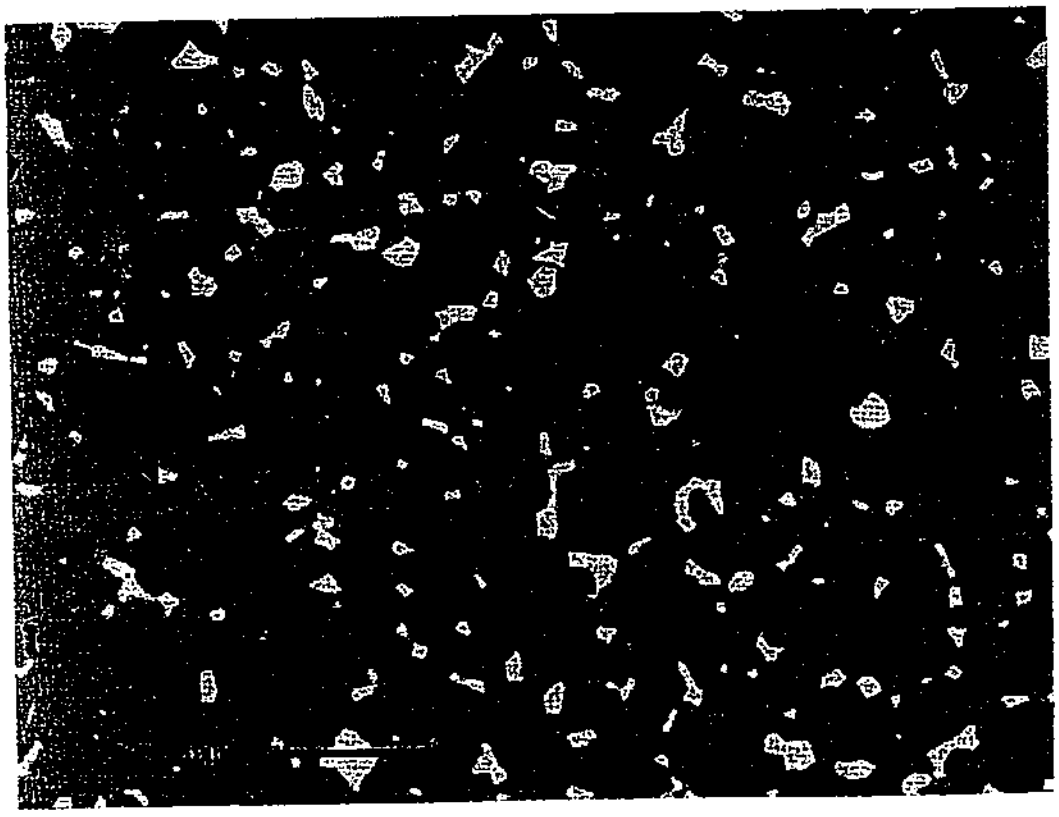

Figure 3.7 Micrograph of the supplied alumina zirconia material prepared by one of the participants

This second part of the round robin was designed to evaluate the participants' abilities to prepare micrographs of suitable quality, and if this was successful, to compare the scatter in results obtained with similar results obtained by the organisers.

The results of the various measurements were to be gathered on a reply form, Appendix 1, by each participant and returned for evaluation together with micrographs and figures made during the task.

The statistical evaluation of the results, consisting of sets of n experimental datapoints, were described with the following simple statistical parameters [4], which were deemed adequate for the purpose:

Mean:

$$\bar{x} = \sum_{i=1}^{n} x_i$$

Standard deviation:

$$s = \sqrt{\sum_{i=1}^{n} \frac{(x_i - \bar{x})^2}{(n - 1)}}$$

Range:

$$R = x_{max} - x_{min}$$

Scatter:

$$\Delta x_{max} = | x - \bar{x} |_{max}$$

Coefficient of variation (relative error of result):

$$C_v = \frac{s}{\bar{x}}$$

The confidence level (95%) was also determined as the confidence on the mean result (approximately ± 2 ±× standard error of the mean).

4. Preliminary examination

Background research was performed in order to provide reliable background information to set the round-robin conditions and against which to evaluate the scatter on the results gathered from the individual participants. This ensures that the work is performed according to the stereological principles of such measurements.

4.1 Grid size

The computer generated micrograph was used to obtain a proper manual method grid size for all of the micrographs under investigation. To obtain the optimum spacing of the grid relative to the phase grain size, a series of tessellations was made with one of the phases was set to levels of about 50, 40, 20 and 10%. This was expected to be typically the range of the microstructures used for this round robin. The measurements were performed with an automatic image analyser, using a variable grid spacing.

The results of this point counting method were compared with those from the pixel counting method, which is assumed to be the true area fraction. Figure 4.1 reveals that reproducible results are obtained if the total number of intersections for the whole micrograph, is set to at least 200, corresponding to a grid size of less than 0.07 of the image width. This grid size is approximately the grain size. However, in order to ensure this level of reproducibility, the grid size was chosen to be about 0.05 of the image width. In this case the results for apparent area fraction converged within a percent or so of the true area fraction determined by pixel counting, as shown in Figure 4.1.

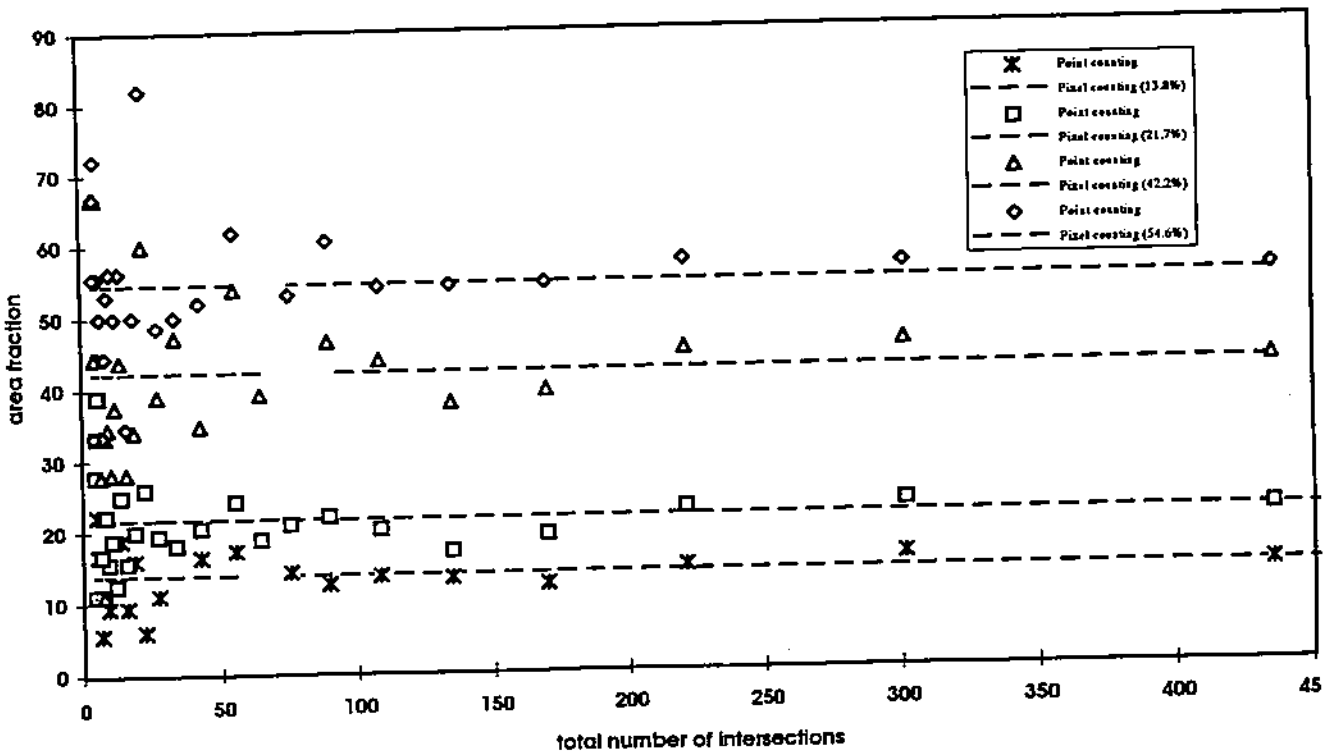

Figure 4.1 Convergence analysis of grid intersection size, showing the variation in analysed volume fraction for four levels of volume fraction in computer drawn 1883x1883 pixel two-phase tessellations as the number of pixels between grid intersections is varied.

Naturally, this grid size is needed to provide the statistics for reproducible measurements because there is a high probability that all grains of each phase will be counted. Any remaining error is mainly caused by the random positioning of the grid and the homogeneity of the phase distribution on the micrograph. Such a condition would not normally apply in practical situation where typically at least three areas would be examined to reduce the risk of a single micrograph not being representative of the section as a whole, it being more essential to count a minimum number of objects in total, rather than completely analyse a single micrograph.

4.2 Homogeneity of the supplied micrographs

The lack of homogeneity of the phase distribution on the micrographs might give an increase in the scatter of results obtained by the participants. This is especially the case when the micrograph is only partially used, as may occur in AIA.

The computer generated 'ideal' micrograph can be used to give insight into the scatter which occurs due to the degree of inhomogeneity. As mentioned before, this micrograph reveals the minimum attainable scatter inherent in the method and can be used as a guideline for the other micrographs. The measurements were performed with both an automatic image analyser, using the pixel counting method, and the manual image analysis technique, using the point counting method. The total image size was 1883 x 1883 pixels.

In order to reveal the sample size at which the volume fraction analysis results are consistent and correct, a so-called convergence analysis was made, requiring the apparent volume fraction to be determined with increasing sampled area. Figure 4.2 shows the results of this convergence analysis. The figure indicates that the volume fraction measurements become converged at a sampled area of approximately 80% of the total sample area.

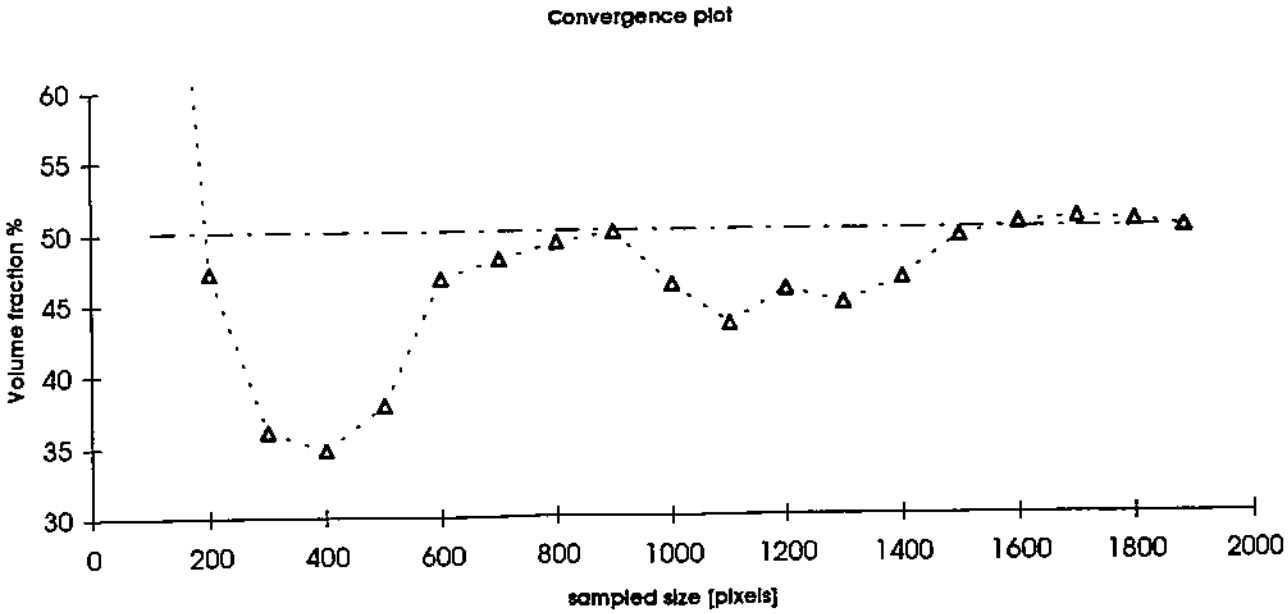

Figure 4.2 Convergence analysis of used micrograph area showing the apparent volume fraction as function of (square) pixel area.

In cases in which the micrograph is only partially used, this could lead to a deviation of the results from the true mean of about ± 10%. However, this convergence analysis is direction dependent due to the use of a fixed starting point and direction of sample size propagation. The converged sampled size could be dependent on the starting point, but nevertheless it is clear that the scatter is likely to be significantly influenced if the micrograph is only partially used, a possibility if participants had only limited pixel number capability.

A similar result is obtained using both the manual analysis method as the automatic analysis starting from the centre of the micrograph, see figure 4.3. In this case the number of intersections and grid size is kept constant, whereas the magnification of the area of interest of the micrograph was varied.

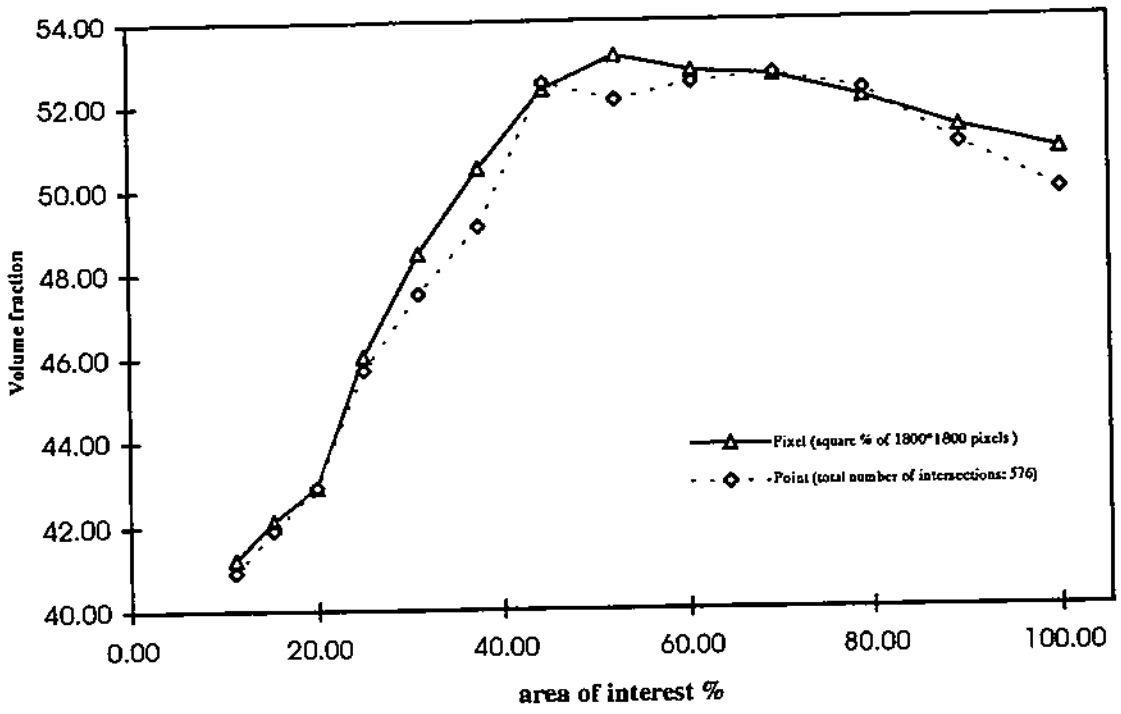

Figure 4.3 Convergence analysis of used micrograph area showing the apparent volume fraction as function of area of interest.

In order to reveal the phase distribution, independently of the starting point and direction, an analysis was made using a fixed frame which was placed, more or less randomly, on the micrograph. Two frequently occurring AIA frame sizes were used, namely 512 x 512 and 1024 x 1024 pixels. A total of 29 sections was made with the 1024 x 1024 image size and 64 with the 512 x 512 image size. The results of these measurements are shown in Figure 4.4. Both measurements are revealing a clearly inhomogeneous phase distribution.

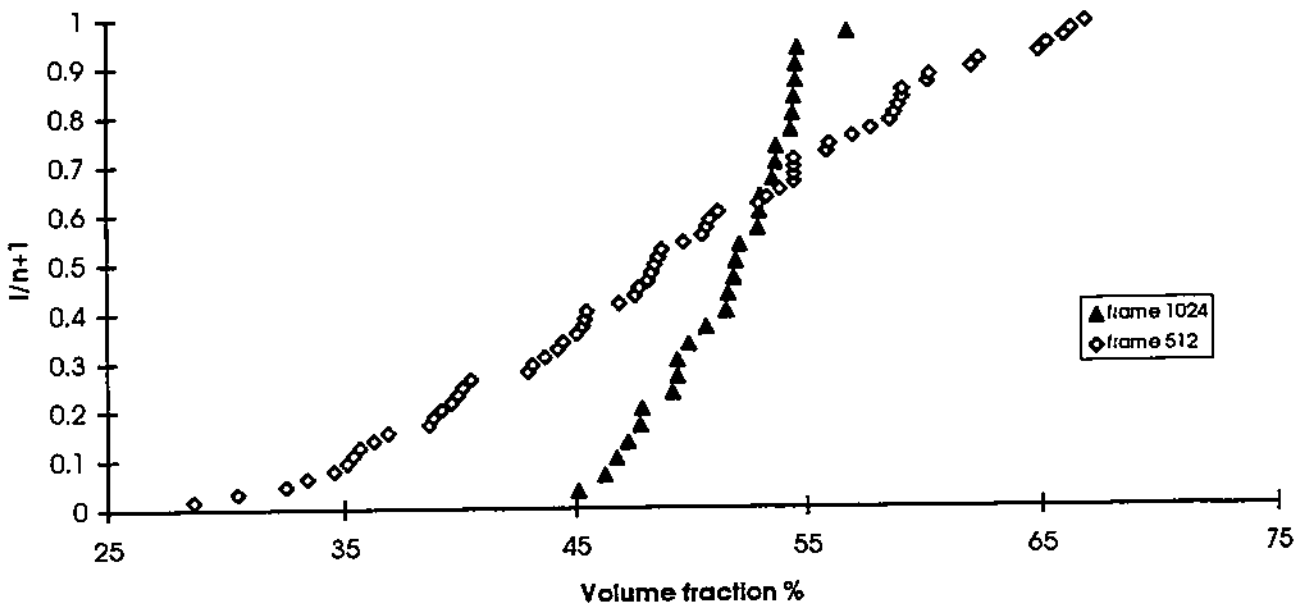

Figure 4.4 Ranked plot of the apparent volume fraction results from the random position of 1024x1024 and 512x512 pixel areas of the 1883x1883 tessellation image showing the scatter in results.

Summarising, it is concluded that partial analysis of the micrograph leads to an increase in the scatter of the volume fraction results. Moreover, a sample size of 1024 x 1024 pixels is approximately 30% only of the total supplied image area, and results in a potential scatter of 5%.

4.3 Homogeneity of the supplied alumina/zirconia sample

An analysis of the alumina/zirconia ceramic has been made by AIA to establish the spatial variability of the volume fractions in order to permit later assessment of the results from individual participants. Scanning effects, intensity drifts, topographic contrast effects (including grain boundaries) and detector noise were minimised by using BSE images obtained with an SEM controller set to capture five pixel repeats with frame averaging over twenty scans. Using 77 such images from different areas of the material, the distributions of phase and pore volume fractions have been assessed.

Figure 4.5 shows a typical grey level histogram for a single image expanded to fill the intensity range 0 to 255. Porosity is clearly defined at zero, the central peak is alumina, and zirconia appears in the range 180-255. Volume fractions were determined by placing markers between the peaks and counting the number of pixels between the markers.

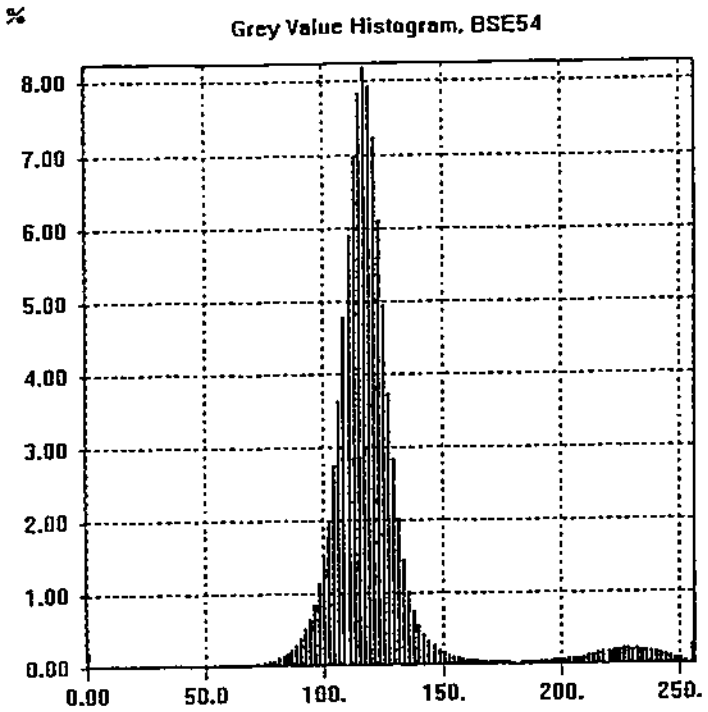

Figure 4.5 Distribution of pixel intensities for a single BSE image of the alumina/zirconia material expanded to a range of grey levels from 0 to 255.

Figure 4.6 summarises zirconia volume fraction data for all images, indicating that the distribution of zirconia is not homogeneous, but varies by typically a factor of two. Single results from individual participants can be compared with this range.

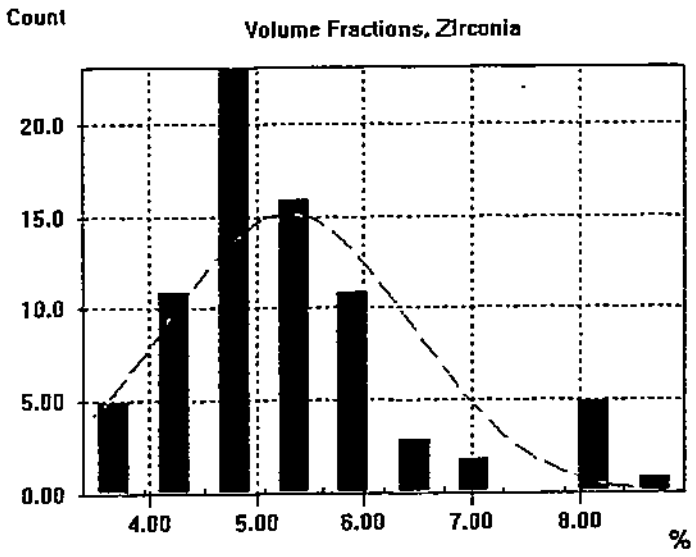

Figure 4.6 Distribution of volume fractions of zirconia from BSE images of 77 different areas.

5. Round robin results analysis

In this section the results of the volume fraction round robin are gathered and discussed. Altogether, 27 participants from Asia, USA and Europe responded to this round robin. Appendix 2 displays the measurement condition of the individual participants. Furthermore, Appendix 3 shows the complete results of the individual participants for each part of this phase volume fraction round robin.

5.1 Manual image analysis

The results of the manual analysis method consist of the number of intercepts lying over each phase or pore. Normalisation of this number of intersections for each phase by the total number of intersections results in the various volume fractions.

The scatter of results for each participant is visualised using the calculated volume fraction of one phase as function of the total number of intercepts of all phases, including pores. Furthermore, in order to represent the data distribution, the volume fractions are put in ascending sequence, numbered from $i = 1$ to n, where n is the total number of participants. The data distribution is now represented by the ascending volume fraction as function of i divided by $(n + 1)$.

5.1.1 Part 1 : Supplied micrographs

The ideal computer generated microstructure, micrograph A, shows a scatter in the results of about 3% with a standard deviation of 1.5% (Table 5.1). This is, as mentioned above, the minimum likely attainable error for these types of measurements.

Table 5.1 Volume fraction results of micrograph A, using the point counting method.

Micrograph A	Mean	Standard deviation	Range	Scatter	Confidence level (95%)	Coefficient of variation	Count
% Light phase	49.0	1.5	5.9	3.2	0.56	3.0%	26
% Dark phase	51.0	1.5	5.9	3.2	0.56	3.0%	26
% Porosity							
Compensated for possible phase reversal							
% Light phase	48.5	0.9	2.7	1.4	0.34	1.9%	25
% Dark phase	51.5	0.9	2.7	1.4	0.34	1.9%	25
% Porosity							

According to Figure 5.1, the data have a normal distribution and there is no relation between the scatter and the total number of intercepts used (Figure 5.2). The scatter is, as mentioned in section 4, mainly caused by the positioning of the grid and the degree of homogeneity of the phase distribution. However, it is quite possible that the results of the two phases were exchanged on the reply form, because the volume fractions of these phases are almost equal. Namely, 5 of the 26 participants determined a volume fraction which was larger for the light phase than for the dark phase, compared with the true result in which the light phase was in a slightly lower proportion than the dark phase. If it is assumed that the phase identity was switched inadvertently by these 5 participants, and this switch is corrected, then the scatter drops to less than 2% and the standard deviation to approximately 1%[2].

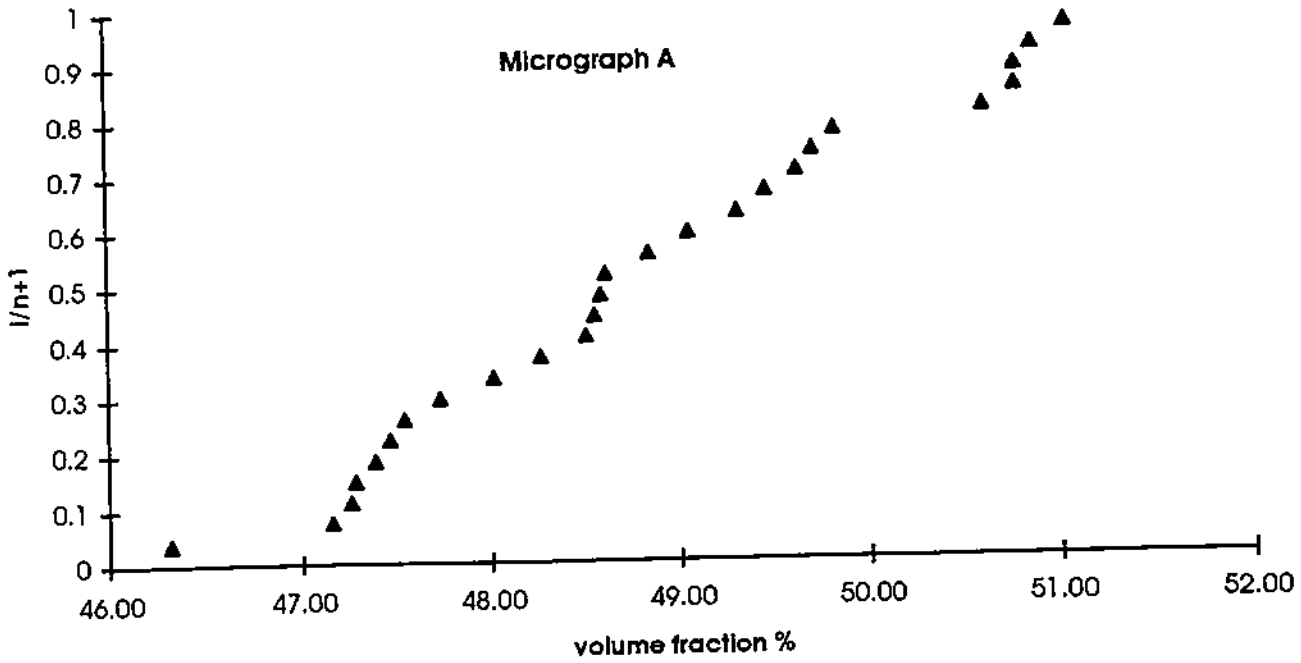

Figure 5.1 ***Ranked plot of all results of the manual determination of the volume fraction of the light phase in Micrograph A. The scatter results from random positioning of the grid.***

[2] The appropriateness of making this compensation may be questioned. While this can definitely happen with automatic image analysis owing to the need to make contrast reversals when delineating relevant phases (as happened unintentionally during setting up this round robin) the risk of this happening with the manual method is possibly slight but not readily traceable.

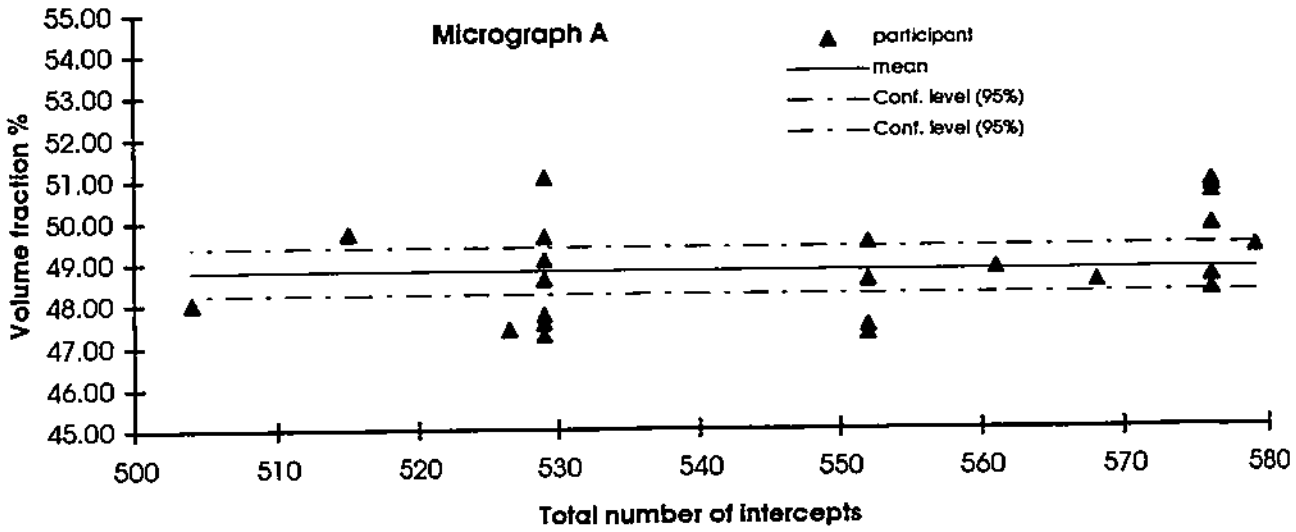

Figure 5.2 Apparent volume fraction of the light phase in Micrograph A as function of the number of intersections counted by participants.

The scatter for the barium titanate type ceramic, micrograph B, increases relative to micrograph A, to 7%, with a small increase of the standard deviation, see Table 5.2. The large range of the results is mainly due to the results of one participant, Figure 5.3. For the barium titanate micrograph, as well as the computer generated micrograph this participant reported a significantly smaller volume fraction than the average, but the number of intercepts used was not provided on the reply form. If the results of this participant are left out of consideration, the scatter decreases, and one obtains approximately a scatter of 4% with a standard deviation of 2%.

Table 5.2 Volume fraction results of micrograph B, using the point counting method.

Micrograph B	Mean	Standard deviation	Range	Scatter	Confidence level (95%)	Coeffi-cient of variation	Count
% Light phase	59.2	2.5	11.1	7.1	0.97	4.2%	26
% Dark phase	39.7	2.0	7.5	3.9	0.78	5.0%	26
% Porosity	1.1	1.8	9.3	8.2	0.69	#	26
Compensated for a single abnormally low result							
% Light phase	59.5	2.1	6.9	3.2	0.80	3.5%	25
% Dark phase	39.8	2.0	7.5	4.0	0.80	5.0%	25
% Porosity	0.7	0.7	2.6	1.9	0.27	#	25

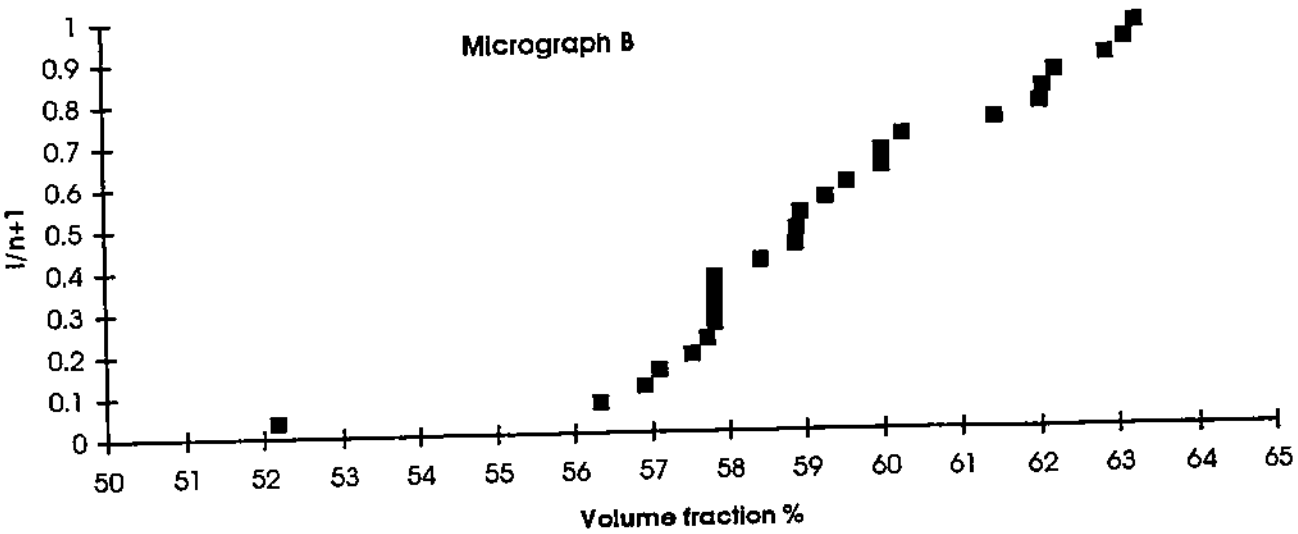

Figure 5.3 Ranked plot of all results of the manual determination of volume fraction of the light phase in Micrograph B.

It seems, according to Figure 5.4, that the mean and the scatter possibly decrease with increasing total number of intercepts. This is probably primarily due to the positioning of the grid, and to an increase in inhomogeneity of the microstructure from that shown by micrograph A. Furthermore, the increased difficulty of phase designation due to the poorer clarity of grain boundaries and the presence of an extra phase, namely the pores, are probably further but minor contributions to this increase of the scatter.

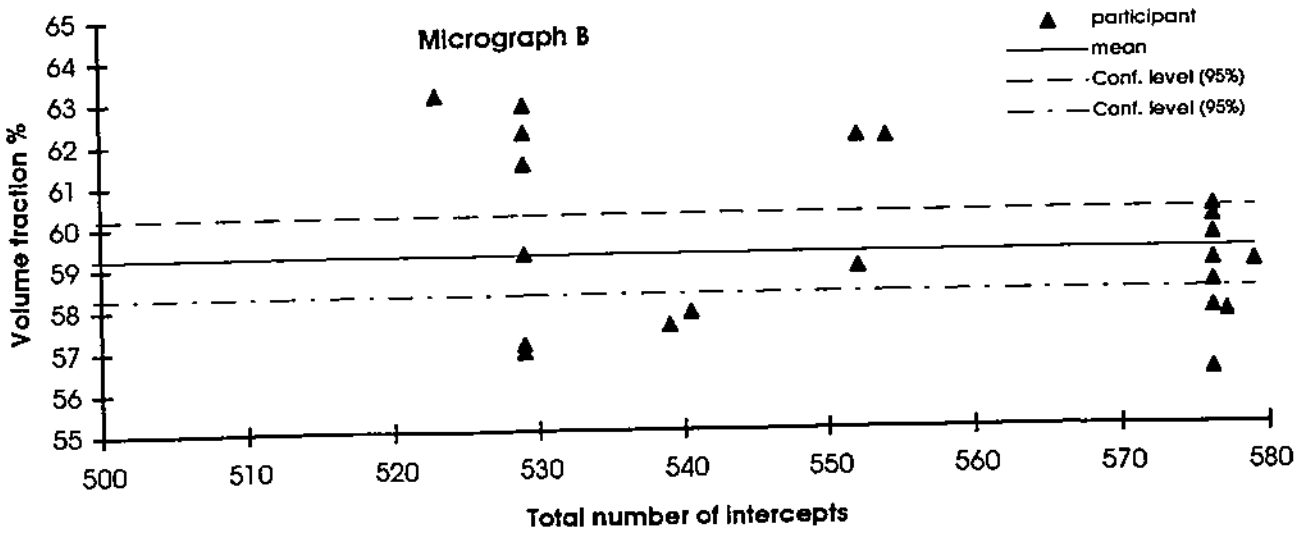

Figure 5.4 Apparent volume fraction of the light phase in Micrograph B as function of the number of intersections counted by participants.

The backscattered electron micrograph C of the alumina/zirconia ceramic has a clear delineation of the phase boundaries. The scatter of the results is about the same as that of the results of the 'ideal' computer micrograph (Table 5.3 and Figure 5.5). The scatter is thought to be due principally to the positioning of the grid relative to the phase distribution. Decisions have to be made by the test operator concerning the nature of pores, and whether bulk material lying somewhat beneath the polished surface but visible within pores should be counted or not.

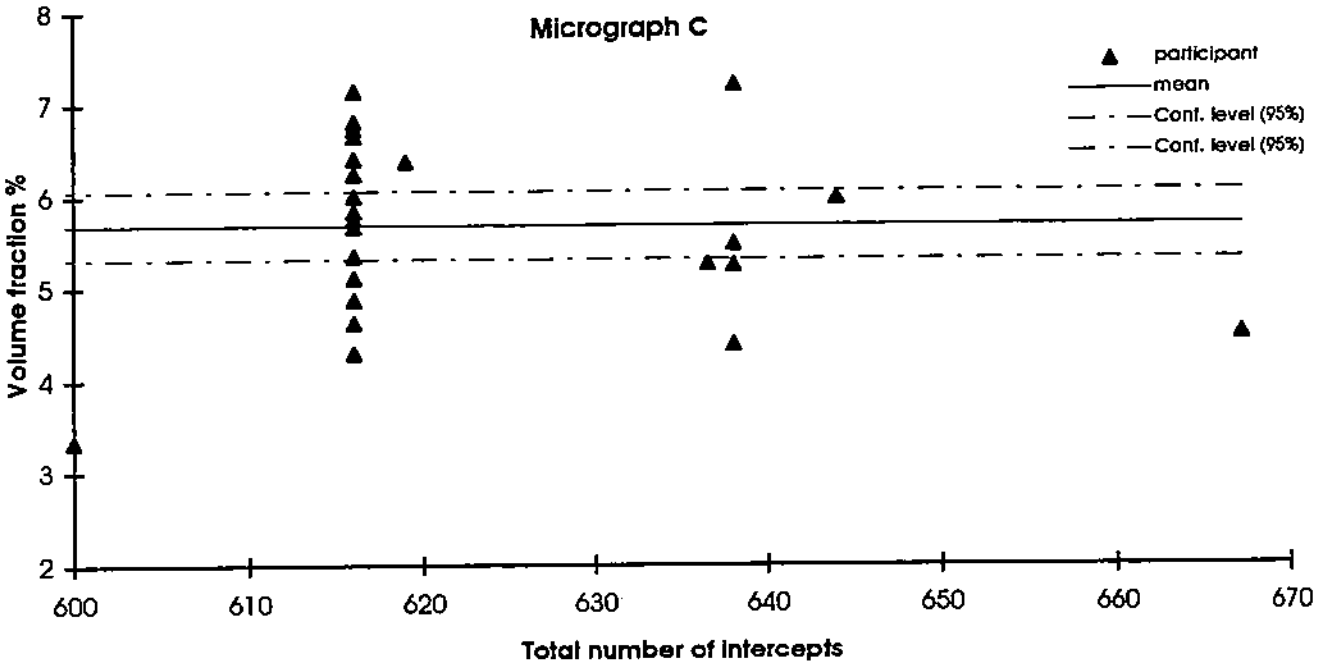

Figure 5.5 Apparent volume fraction of the zirconia (light) phase in Micrograph C as a function of the number of intersections counted by participants.

Table 5.3 Volume fraction results of micrograph C, using the point counting method

Micrograph C	Mean	Standard deviation	Range	Scatter	Confidence level (95%)	Coefficient of variation	Count
% Light phase	5.7	1.0	3.9	2.4	0.37	17.5%	26
% Dark phase	93.3	1.2	5.0	2.9	0.48	1.3%	26
% Porosity	1.0	0.6	2.6	1.6	0.23	#	26
Compensated for low number of counted intersections							
% Light phase	5.8	0.85	2.9	1.5	0.33	14.7%	25
% Dark phase	93.2	1.1	4.2	2.2	0.44	1.2%	25
% Porosity	1.1	0.6	2.6	1.6	0.23	#	25

The results from one participant contributed significantly to the total scatter. The positioning of the grid was probably different or the intercepts on the edges of the micrograph were not taken into account. This possibility arises because the total number of intercepts counted by this participant is about 600, whereas the mean value for all participants comes near to 624 (see Figure 5.5). If the results of this participant are excluded, the scatter drops to approximately 2%, see the lower part of table 5.3.

Compared with the results of micrograph A, the coefficient of variation shows a large increase for the zirconia phase and the pores, whereas that for the alumina phase decreases slightly, Table 5.3. As discussed above, the reason for this is the presence of only small amounts of zirconia and pores. It is most likely that the volume fraction analysis results do not converge for the area described by the micrograph, because the number of intersections is too small for the zirconia phase and the pores. This means that the sampled area should strictly be increased to obtain reliable results for this material.

The influence of the possibility to use the backscattered electron image (micrograph C) to support the analysis of the secondary electron image (micrograph D) is negligible. The results are shown in Table 5.4 and Figure 5.6.

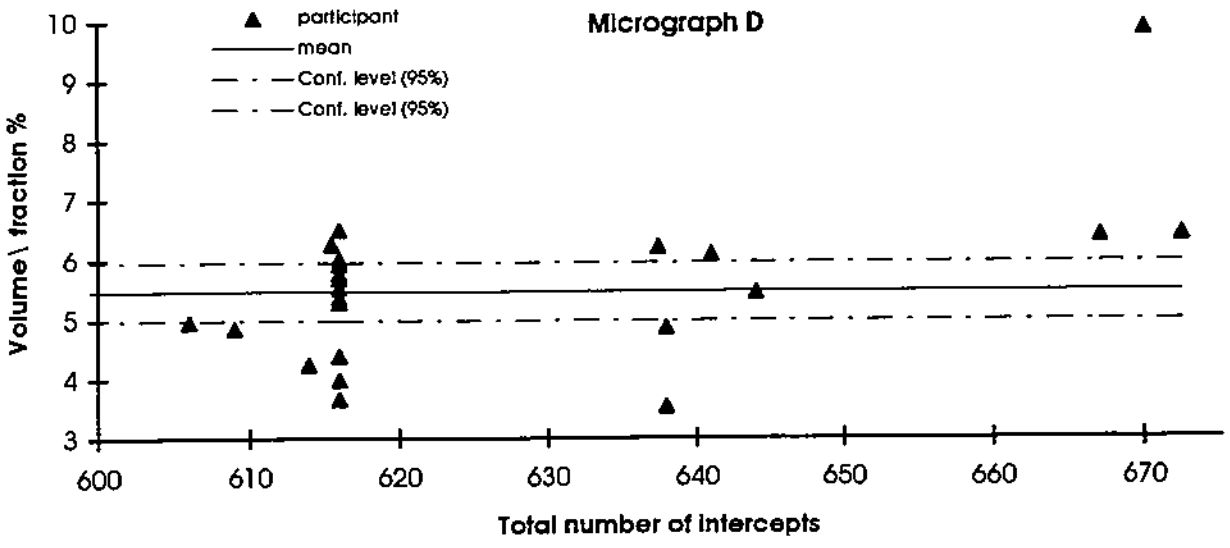

Figure 5.6 Apparent volume fraction of the zirconia (light) phase in Micrograph D as a function of the number of intersections counted by participants.

Again, the measurements of one participant have a large impact on the overall results due to the large deviation from the mean; the volume fraction of the zirconia ceramic is almost twice as large as the mean value (see Figure 5.6). If the results of this participant are excluded, the scatter will decrease to approximately 2% (lower part of Table 5.4).

Table 5.4 Volume fraction results of micrograph D, using the point counting method

Micrograph D (& C)	Mean	Standard deviation	Range	Scatter	Confidence level (95%)	Coefficient of variation	Count
% Light phase	5.5	1.3	6.3	4.3	0.48	23.6%	26
% Dark phase	93.6	1.3	6.0	3.6	0.49	1.4%	26
% Porosity	0.9	0.5	1.6	0.7	0.19	#	26
Compensated by exclusion of high zirconia volume fraction result							
% Light phase	5.3	0.9	4.0	1.8	0.35	17.0%	25
% Dark phase	93.8	1.0	3.0	2.1	0.40	1.1%	25
% Porosity	0.9	0.5	1.6	0.7	0.20	#	25

If the results are compared with those based only on micrograph C (Figure 5.5), they seem to have shifted a little. The mean volume fraction of the alumina phase increases whereas the mean volume fraction of the zirconia phase decreases. However, this is well within the deviation of the results. This becomes more obvious if one looks at the data distribution plot shown in Figure 5.7. The scatter for both data sets remain almost equal.

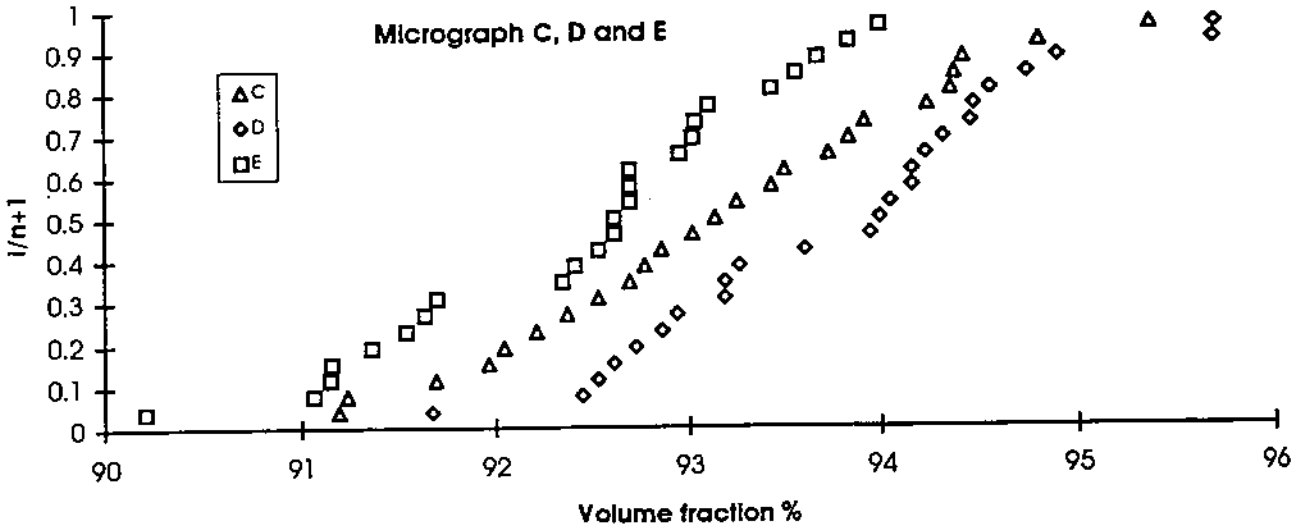

Figure 5.7 Ranked plot of all results of the manual determination of volume fraction of the dark phase in Micrograph C, D and E.

The explanation can be found in the origin of the micrographs. Micrograph C is a smooth backscattered electron image whereas micrograph D is a secondary electron image with a much larger range of contrast for each phase. Micrograph D has mostly a clear and unmistakable delineation of the phase boundaries from topographic detail, but sometimes these phase boundaries are difficult to distinguish due to enhanced electron emission. This happens especially on sharp edges like pore and grain boundaries. This local high intensity can cause significant errors when analysing the phases due to the difficulty in phase recognition. However, the use of both the backscattered electron image as the secondary electron image should make the decisions on distinguishing the phases and phase boundaries easier. Furthermore, the presence of the thermally etched grain boundaries on the secondary electron image is helpful.

The shift in the results of the mean volume fractions between micrograph C and D may genuinely exist. A backscattered electron image has broad gradual phase transitions due to the more in-depth information obtained from the sub-surface microstructure, notably from grains which slope away from the immediate surface. A secondary electron image has sharp phase transitions due to the surface topographic information of the micrograph. The observed shift in results might also be caused by the differences in these phase boundaries because the human eye is more attracted to white on a dark background.

Even for the second secondary electron micrograph of the same material unsupported by a backscattered image (micrograph E) the scatter between participants is not significantly different from that of the other alumina/zirconia micrographs (Table 5.5, Figure 5.8).

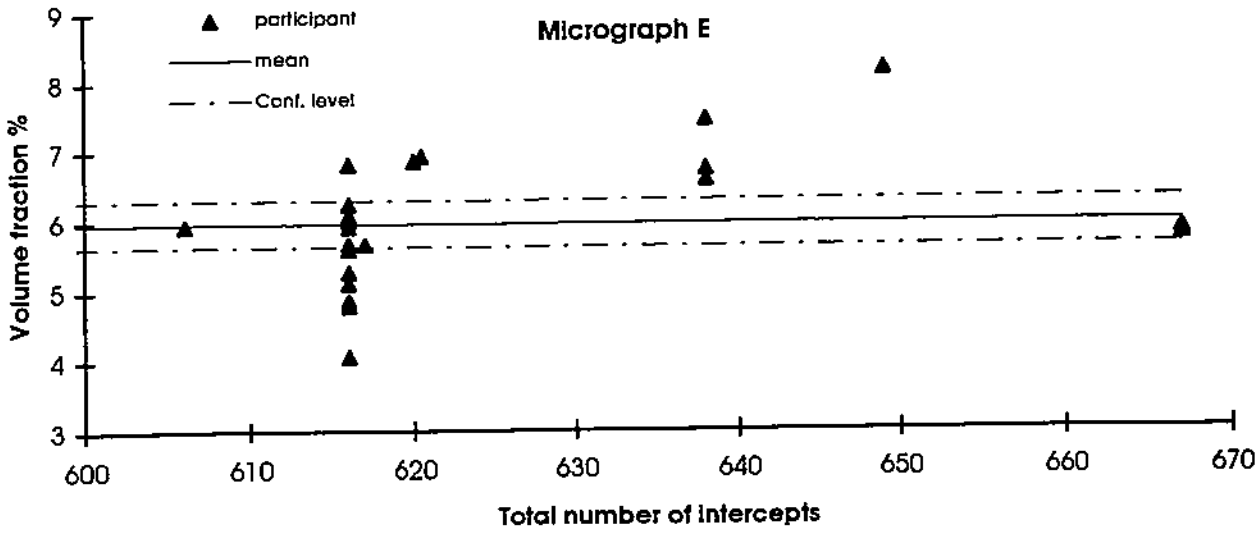

Figure 5.8 Apparent volume fraction of the zirconia (light) phase in Micrograph E as a function of the number of intersections counted by participants.

Table 5.5 Volume fraction results of micrograph E, using the point counting method

Micrograph E	Mean	Standard deviation	Range	Scatter	Confidence level (95%)	Coefficient of variation	Count
% Light phase	6.0	0.9	4.1	2.2	0.33	15.0%	26
% Dark phase	92.5	1.3	5.3	2.9	0.43	1.4%	26
% Porosity	1.5	0.7	3.0	1.8	0.28	#	26

Figure 5.7 shows the data distributions of all three alumina/zirconia micrographs. The shift in the mean volume fractions between micrographs E and C or D is probably due mainly to the effects of area sampling and an indication of material inhomogeneity.

5.1.2 Part 2 : Supplied test sample

The results for the supplied alumina/zirconia test sample using the manual image analysis method, are listed in Table 5.6. The scatter in the results increases compared with the results of the same material used in Part 1, micrographs C to E (Figure 5.9). Figure 5.10 shows the data distribution of the results gathered from the participants.

Table 5.6 - Volume fraction results of the supplied sample, using the point counting method.

Micrograph Part 2	Mean	Standard deviation	Range	Scatter	Confidence level (95%)	Coefficient of variation	Count
% Light phase	8.0	2.1	7.3	4.3	0.94	26.3%	20
% Dark phase	90.5	2.7	8.4	4.9	1.17	2.9%	20
% Porosity	1.5	1.5	6.4	4.8	0.65	#	20

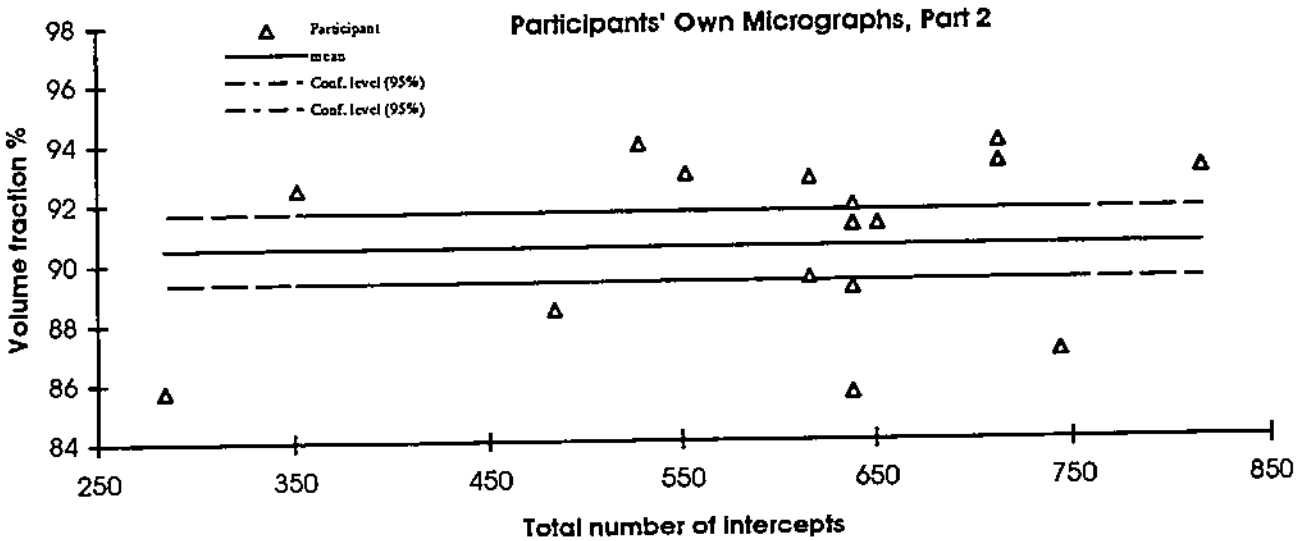

Figure 5.9 Apparent volume fraction of the alumina (dark) phase in Micrograph F prepared by participants as function of the number of intersections counted.

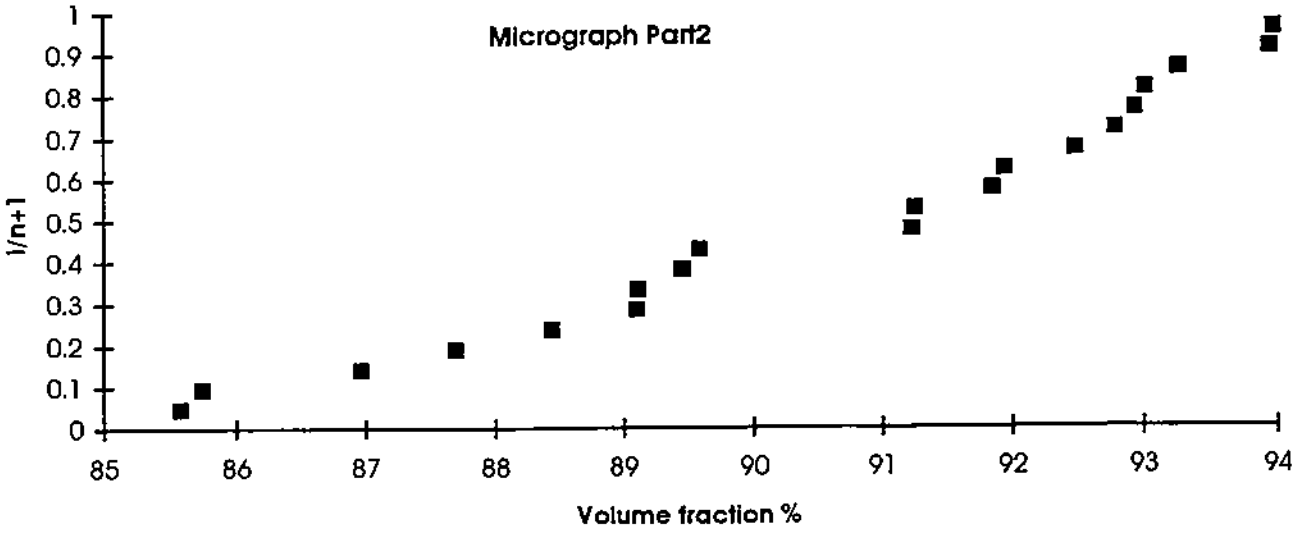

Figure 5.10 Ranked plot of all results of the manual determination of volume fraction of the alumina (dark) phase in Micrograph E.

Looking back at the organisers' results from the 77 BSE images (Section 4), the wide scatter can be expected, and is mainly caused by the inhomogeneity of the sample. The scatter is additionally increased by the variety of practices adopted by the different operators.

Thus, the scatter expected for this part can be considered as a combined scatter typical of the 77 BSE images (Section 4) and the scatter found experimentally in Part 1 for the same material. Furthermore, the increase in scatter might also be influenced by the magnification of the micrograph. As remarked by some participants, the required magnification of 5000 gave some confusion[3]. Some of the participants used a electron microscope magnification of 5000. Others used a lower magnification and enlarged the micrograph until a magnification of approximately 5000 was achieved at almost the same size as the micrographs delivered by the organisers. These two procedures yielded different numbers of observed zirconia grains. In general, the phase volume fractions of the alumina phase appear lower in micrographs taken originally at high magnification, possibly as a result of the eye being drawn to regions with larger than average numbers of secondary phase particles. For instance, one of the participants used magnifications of both 5000 and 1000 for their own sample, which resulted in differences in the subsequently measured volume fractions of the alumina phase of almost 7%. Therefore, to determine the reliability and reproducibility of the results, the magnification selected for the micrographs should be such that the volume fraction analysis converges to the true result. In this respect it is important to count a minimum number of features, irrespective of the number of micrographs that have to be taken to obtain them.

The influence of the sample preparation, which could result in grain tear-out, seemed to be small. This can be concluded if one compares the mean values and standard deviations of the apparent porosity from this Part of the task with the equivalent data from Part 1 using the same material. However, in general the participants reporting a relatively low volume fraction of the alumina phase also reported a higher porosity, suggesting that tear-out was present, affecting primarily the alumina grains, but not so much the apparent zirconia volume fraction.

5.2 Automatic image analysis

The results for the automatic analysis method also comprise the various volume fractions for the different phases and pores. In this method, the human decision making concerning the partitioning of the grey levels to identify the different phases of the image is of prime importance. The overall results of the volume fraction determinations for each phase, including porosity, are shown in the following tables and figures.

5.2.1 Part 1 : Supplied micrographs

Results for ideal computer generated microstructure showed a scatter of approximately 6% (Figure 5.11) with a standard deviation of 3% (upper part of Table 5.7). This should be the minimum attainable error for these types of measurements. In this case however, the scatter is mainly introduced by the finite width of the grain boundaries. Some of the participants, 8 out of 23, have counted the grain boundaries as a separate 'phase'. This is more or less correct if

[3] In hindsight, the instructions contained some ambiguities concerning magnifications, for which the organisers apologise. However, this does emphasise the difficulty in providing explicit instruction concerning appropriate magnifications to be used for this type of analysis.

only the boundaries between the different 'phases' were counted (but not those between similar phases), and counted half for each phase. To provide the minimum attainable scatter one can take these effects into account and adjust the relevant sets of results in this sense. The most obvious manner is to divide the grain boundaries according to the percentage of the phases present, see Appendix 3. This reduces the scatter to about 5% (centre part of Table 5.7).

Table 5.7 - Volume fraction results of micrograph A, using the pixel counting method

Micrograph A	Mean	Standard deviation	Range	Scatter	Confidence level (95%)	Coefficient of variation	Count
% Light phase	47.8	2.5	10.5	6.1	1.02	5.0%	23
% Dark phase	49.2	3.0	9.4	5.0	1.22	6.1%	23
% Grain boundaries	3.0	4.2	11.7	8.7	1.72	#	23
Compensated for known grain boundary effects							
% Light phase	49.3	1.8	8.1	4.6	0.75	3.7%	23
% Dark phase	50.7	1.8	8.1	4.6	0.73	3.6%	23
% Grain boundaries	0						
Compensated also for potential error due to contrast inversion							
% Light phase	48.8	1.5	4.2	2.9	0.61	3.1%	23
% Dark phase	51.2	1.5	4.2	3.0	0.59	2.9%	23
% Grain boundaries	0						

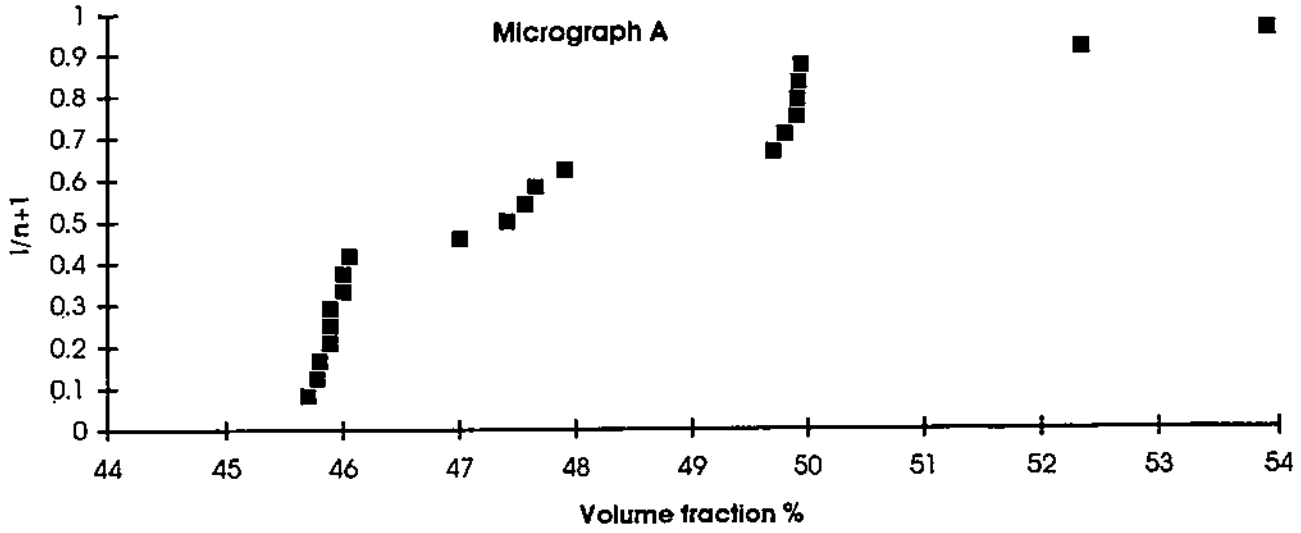

Figure 5.11 Ranked plot of results for the AIA determination of the volume fraction of light phase in Micrograph A. The data fall into groups which appear to depend on the technique used for inputting the original file into the analyser.

Furthermore, as mentioned above for the manual method, the possibility exists that the results for the two phases are exchanged on the reply form. In the present case, two participants have determined a volume fraction of the light phase which is larger than the volume fraction of the dark phase. One of them did not use the total image area, which could be an alternative explanation for the volume fractions found. Thus, if one takes this possible exchange into account, the scatter decreases to 3% (bottom part of Table 5.7).

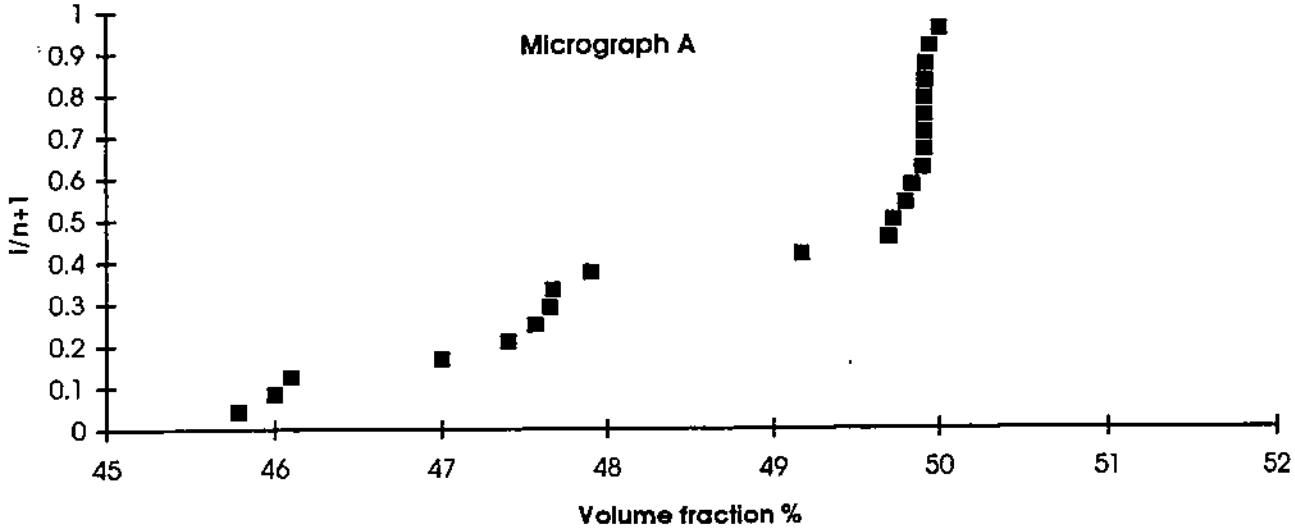

Figure 5.12 As Figure 5.11 but compensated for inadvertent reversal of phase 'colour' identification in AIA.

Figure 5.12 shows the data distribution of the compensated results. Theoretically, one would expect, for this micrograph and with this method, a scatter which is reduced to zero. The partitioning of the grey value levels should not be a problem because they have unique values rather than a spectrum. However, the obtained scatter appears to be caused by re-sizing the image, by not using the total image size, or by converting it into another format. Re-sizing the image means a change in the pixel resolution which will result in reformatting the pixels and, depending on the software performing this function, may result in averaging of grey levels or changing grain boundary widths. Typical image sizes used by participants in this round robin are 512 x 512 and 1024 x 1024. The scatter changes, also by typically up to 2%, due to changes in boundary contrast and width. Furthermore, an increase in the scatter is obtained if one uses only a section of the micrograph area. This is due to the inhomogeneity of the phase distribution, as mentioned before. The image conversion into another format can also lead to a shift of the pixel coverage area, especially in cases in which a video scanner is used.

The scatter for the barium titanate type ceramic (micrograph B, Figure 5.13) increases compared with the manual method, in this case to almost 11%, with a comparable increase in the standard deviation (Table 5.8).

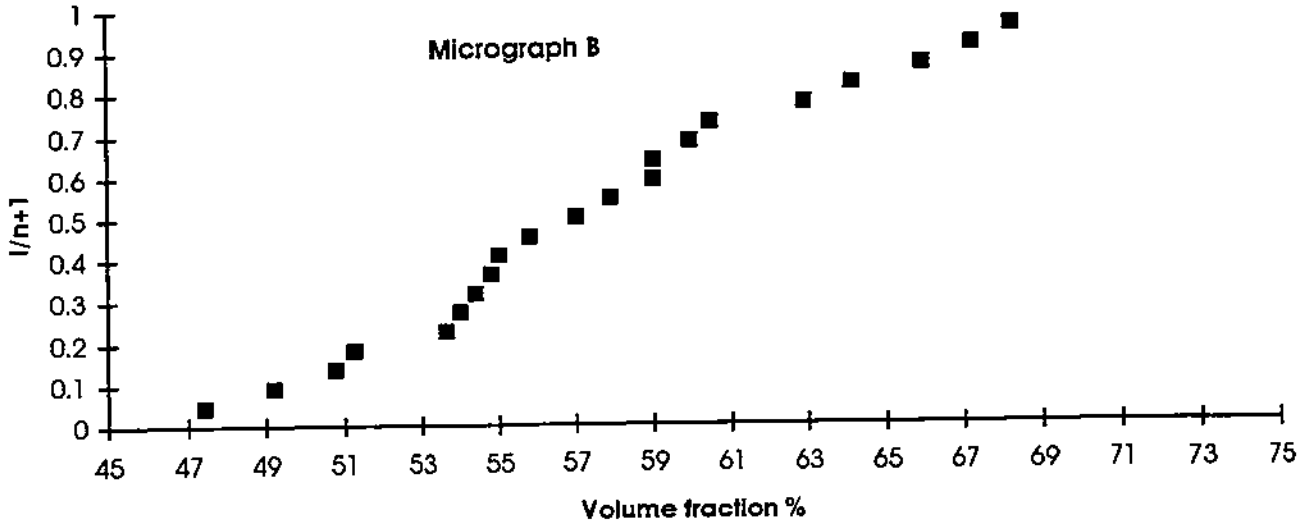

Figure 5.13 Ranked plot of results for the AIA determination of volume fraction of light phase in Micrograph B.

Table 5.8 - Volume fraction results of micrograph B, using the pixel counting method

Micrograph B	Mean	Standard deviation	Range	Scatter	Confidence level (95%)	Coefficient of variation	Count
% Light phase	57.5	5.8	20.8	10.7	2.49	10%	21
% Dark phase	40.6	5.2	17.2	9.1	2.24	12.8%	21
% Porosity	1.9	2.3	7.9	6.0	0.99	#	21

The increase in the scatter is mainly due to the difficulties of phase differentiation through the need to partition the grey levels of the digitised image. The presence of an extra phase, namely the pores, is probably a second, but minor, contributor to this increase of the scatter. Furthermore, the scatter itself is caused not only by the partitioning of the grey levels, but also by resizing, sectioning, and conversion of the image to another format, as mentioned above.

The results for the alumina/zirconia type ceramic (micrograph C) reveal a comparable scatter (Figure 5.14 and Table 5.9) to that for the 'ideal' micrograph. This is probably due to the good contrast between the phases on the micrograph, which makes it easier to differentiate the phases via grey level distributions. However, as for the manual method, the coefficient of variation increases for the zirconia phase and the pores due to poor statistics of the small volume fractions involved.

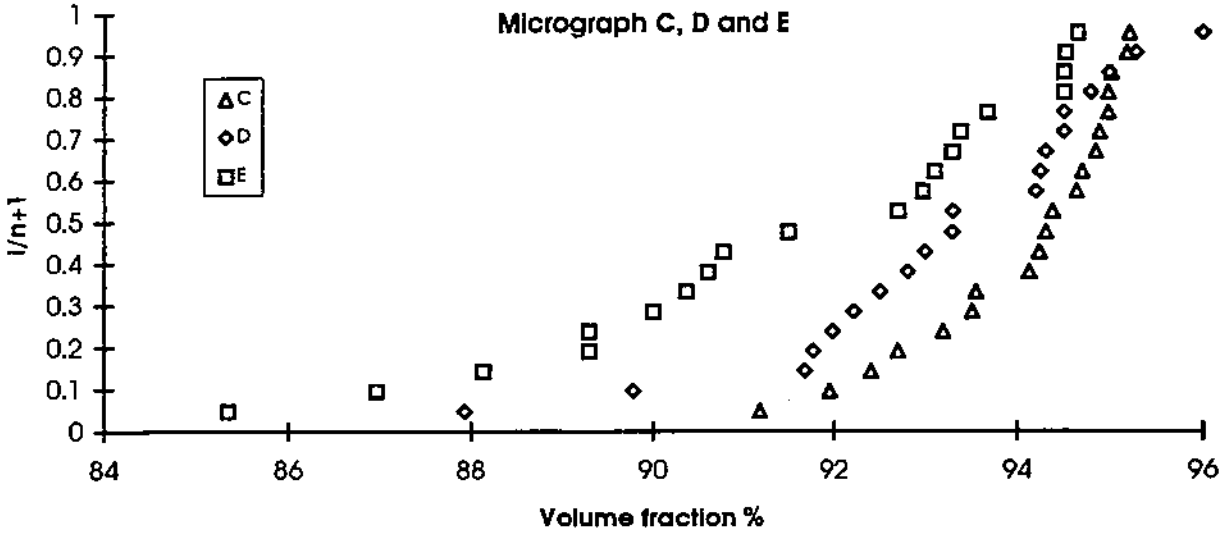

Figure 5.14 Ranked plot of all results of the AIA determination of volume fraction of the dark phase in Micrograph C, D and E.

Table 5.9 Volume fraction results of micrograph C, using the pixel counting method

Micrograph C	Mean	Standard deviation	Range	Scatter	Confidence level (95%)	Coefficient of variation	Count
% Light phase	4.9	0.8	2.7	2.2	0.51	16.3%	20
% Dark phase	94.0	1.2	4.1	2.8	0.35	1.3%	20
% Porosity	1.1	0.8	3.2	2.2	0.33	#	20

Despite the possibility of using the backscattered electron image, micrograph C, to support the interpretation of the secondary electron image, micrograph D, an increase of the scatter of results was found (Figure 5.14 and Table 5.10). This is probably due to the difficulty of separating porosity in the grey value distribution. It is most likely that the participants did not, or could not, combine the information available in the two micrographs. This is probably because most automatic analysers can deal with only one micrograph at a time, and human intervention is needed to provide the interpretative cross-link. In general, the partitioning of the grey values of a secondary electron image is more complicated compared with processing a backscattered electron image. Although there are risks of detecting and incorrectly counting subsurface bright phases, a backscattered image has a clear contrast between the phases and very limited contrast inside the phases, whereas the secondary image can see, for example, phase contrast at the bottom of shallow pores. This is probably a reason for the increase of scatter as shown in Figure 5.14. The decisions which have to be made concerning the size of the pores and the counting of the phases lying somewhat beneath the immediate surface are more clear-cut for the backscattered image than for the secondary image.

Table 5.10 - Volume fraction results of micrograph D, using the pixel counting method.

Micrograph D	Mean	Standard deviation	Range	Scatter	Confidence level (95%)	Coefficient of variation	Count
% Light phase	6.0	2.0	7.6	4.7	0.87	33.3%	20
% Dark phase	93.2	1.9	8.1	5.3	0.85	2.0%	20
% Porosity	0.8	0.5	1.8	1.2	0.24	#	20

Furthermore, the possibility of 'misinterpretation' of the phases and the phase boundaries due to the bright halo effects which occur in the regions of enhanced secondary electron emission, as mentioned in Section 5.1.1, might have led to a further increase in the scatter. The phase which has a similar grey value to the halo, in this case the light-coloured zirconia, appears to be present at a higher level. This halo effect can thus cause significant errors if the adjacent grains cannot be correctly assigned to a certain phase.

Results from micrograph E, the second secondary electron image, showed a slight increase in scatter compared with the first, micrograph D (Figure 5.14 and Table 5.11). This increase is probably due to the wider range of contrast in the image and the higher level of the porosity, together with the associated errors.

Table 5.11 - Volume fraction results of micrograph E, using the pixel counting method

Micrograph E	Mean	Standard deviation	Range	Scatter	Confidence level (95%)	Coefficient of variation	Count
% Light phase	7.1	2.3	7.9	5.6	1.01	32.4%	20
% Dark phase	91.5	2.7	9.3	6.2	1.19	3.0%	20
% Porosity	1.2	1.0	4.0	3.1	0.42	#	20

Furthermore, for all three alumina/zirconia micrographs, the scatter itself is caused not only by the partitioning of the grey levels, but also by re-sizing, by sectioning, or by converting the image to another format, as mentioned before.

5.2.2 Part 2 : Supplied test sample

The results for the supplied alumina/zirconia sample using the automatic image analysis method are listed in Table 5.12. The scatter of the results (Figure 5.15) is larger than shown by the results of micrographs C to E (Figure 5.14)

Table 5.12 Volume fraction results of the supplied sample, using the pixel counting method

Micrograph Part 2	Mean	Standard deviation	Range	Scatter	Confidence level (95%)	Coefficient of variation	Count
% Light phase	7.3	2.7	9.9	6.7	1.37	37.0%	15
% Dark phase	91.0	4.2	13.2	9.2	2.11	4.6%	15
% Porosity	1.7	2.2	8.8	7.1	1.12	>100%	15
Compensated by exclusion of high zirconia or porosity volume fraction result							
% Light phase	6.2	1.5	4.9	2.8	0.84	25%	12
% Dark phase	92.8	1.7	5.9	3.7	0.92	1.7%	12
% Porosity	0.9	0.8	2.3	1.4	0.44	89%	12

If the results of the micrographs prepared by the participants are compared with those from the 77 BSE images prepared at NPL (see Section 4), as well as with the results from Part 1 using the same material, the observed increase in scatter is to be expected. This is probably due in part to the variations in preparation techniques, but mainly to the inhomogeneity of the sample and the variations in differentiation of the phases and pores achieved by the participants. Another factor of prime importance to the achievement of consistent results was the magnifications of the micrographs. It is most likely that the volume fraction analysis results are not totally converged for the sample area used by many of the individual participants, which has resulted in an increase of scatter.

For instance, two participants measured volume fractions of about 86% and 12% for, respectively, the alumina and zirconia phases, which is a deviation of about 5% with respect to the mean value from all participants. Furthermore, the appearance of the bright halo like effects causes maybe another contribution to this shift.

The influence of the sample preparation techniques, which could result in grain tear-out, is thought to have been small by inspection of the detail of the micrographs. This can also be concluded if one compares the mean values and the standard deviations of the porosity (Table 5.12). Only the two participants recording a low apparent volume fraction of the alumina phase of about 82% (see Figure 5.15) measured relatively high porosities, namely 3.5% and 8.8%.

The scatter and the standard deviation decrease to less than approximately 4% and 2%, respectively, if the results of the participants with a high volume fraction of zirconia and porosity are excluded, see Table 5.12. However, it should be noted that the exclusion of three participants means a decrease of 20% on the total number of results.

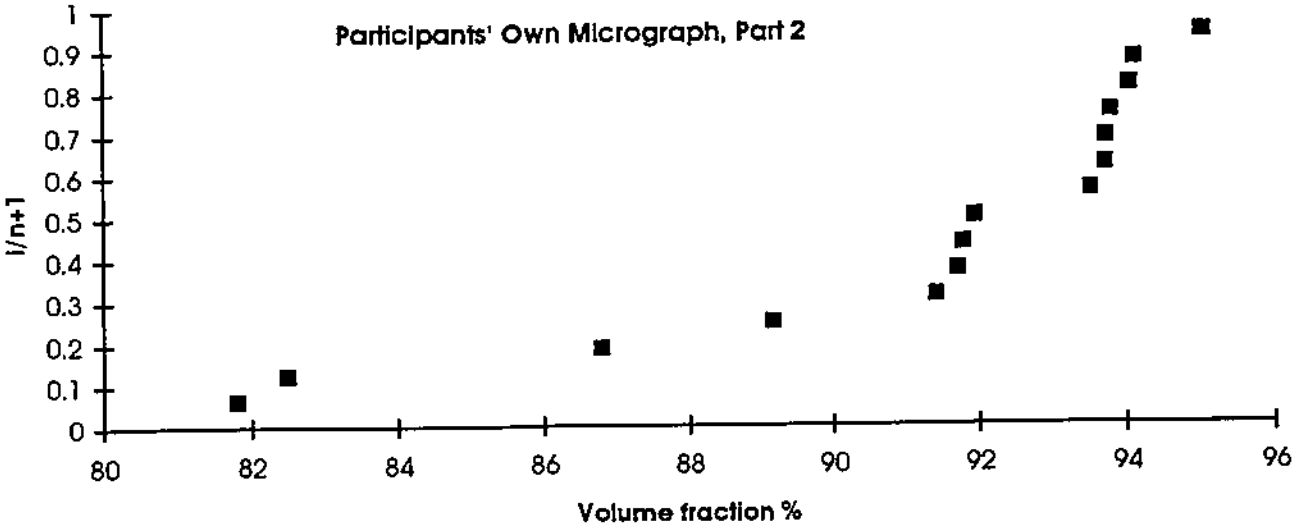

Figure 5.15 Ranked plot of results for the AIA determination of volume fraction of dark phase in Micrograph F prepared by the participants.

6. Method, Volume Fraction and Scatter

The volume fractions for both the manual and the automatic image analysis are determined by counting a certain number of points or areas for each phase, which are related to the total numbers of all phases. In the case of manual analysis, this counting method is set by the number of intersections, while for automatic analysis this is set by the number of pixels.

In order to predict the number of test points that is required to achieve a certain precision it is found in literature [2] that the number of test points, N, is related to the volume fraction, V_a, as:

$$N = \left(\frac{z}{d}\right)^2 \cdot \frac{1 - V_a}{V_a}$$

The required precision is defined by the confidence interval, d, and the acceptable error probability that a estimate may fall outside this interval, z, which is the abscissa of the normal curve which cuts off an area fraction of the probability at the tails. The values of z can be obtained from the general statistical tables.

In general a 95% probability, whereby z is approximately 2, giving a confidence interval, d, of 10% of the true mean, is used to describe a good statistical result. For a volume fraction of 50%, as in the tessellation micrograph, a number of about 400 intersections is required. If this volume fraction becomes 10% or less, e.g. the zirconia phase and the porosity in the alumina/zirconia, the total number of points should be larger than 3600 points. This amount will not be a problem for the automatic analysis, but the total amount of intersections for the manual analysis is set to only approximately 600 points. For volume fractions of less than 10% this results in a confidence interval of more than 30%, up to 60% for volume fractions of a few percent. Therefore, the total area of interest, or the number of individual areas, should be enlarged to obtain consistent results in the case of small phase volume fractions.

However, in practice an ideal homogeneous sample seldom exists. This implies that although it is possible to determine the microstructure parameters of one micrograph within a certain precision, it is recommended that the microstructure parameters are determined by using several micrographs of the same sample and averaging the accumulated result.

Looking back at the results of the manual analysis, one could therefore have expected the obtained large scatter on the results, especially for the low volume fraction such as pores and zirconia. However, the confidence interval of the results seems to be in good agreement with the equation above. In fact the scatter in results between the participants is of a size similar to the level of precision predicted by the above equation.

The larger scatter of the automatic analysis results appears to be caused mainly by the partitioning of the grey valuc levels.

Certainly, as mentioned before, the positioning of the grid, the phase/porosity designation, the use of only a section of the supplied micrographs, the re-sizing of the image, and image conversion also contribute to an increase of the scatter.

The problem of measuring a small amount of phase or porosity, was already stated in an earlier CEN/VAMAS round robin [1], whereby the scatter of the results was of the same magnitude as in this round robin.

Although the results of the manual analysis reveal this technique to be apparently better than the results of the automatic analysis, the decision of which method is more convenient for a certain microstructure analysis depends also of the amount of work. The manual method is probably more convenient for analyses of a few micrographs, while the automatic analysis is more efficient for analyses of a large number of micrographs with a similar set-up concerning the preparation and processing of the microstructural image, provided that the images contain negligible contrast ambiguities which require manual intervention.

7. Concluding remarks

A round robin has been designed, executed and analysed to reveal the scatter in results occurring between different laboratories in the determination of the volume fraction of phases, including pores, in multiphase advanced technical ceramics. Twenty-seven participants from Asia, Europe and the USA took part. The returned results have been analysed in detail, from which a number of conclusions can be made:

1. In general, both the manual and the automatic image analysis methods reveal statistically consistent and reproducible results.

2. The results for the manual method are outstandingly consistent for all the micrographs supplied; the standard deviation of the volume fraction results is within ± 2.5% (expressed as a phase volume fraction), and the 95% confidence interval on mean values is less than ± 1.0%. These results are sufficiently promising that the basis for a standard can be prepared with confidence, endorsed by the results of this round robin.

3. The automatic analysis method shows that for micrographs with clear contrast and distinguishable phases (micrograph A, C, D and E), the scatter of the volume fraction of major phases is about ± 4% (expressed as a volume fraction) with a standard deviation of less than ± 2%. The numerical characterisation of microstructures seems to yield more-consistent results if they are correctly interpreted by the human eye rather than analysed using completely automatic means, especially for complex microstructures. Greater scatter was obtained for a micrograph with significant variations in grey level across each phase.

4. The scatter in the results of the manual method is mainly produced by the positioning of the grid and by the distribution of the phases. The scatter of the automatic method is mainly produced by the increased difficulties of differentiation of the phases and the need to partition the overlapping distributions of grey levels for each phase. Furthermore, the scatter has been found to increase due to practical factors such as re-sizing the image, converting it to another format, or using only a part of the area of the micrograph. The re-sizing of the image results in a change of the resolution which causes the pixels to re-format. Conversion of the image into another format can also lead to a shift of the pixel size, especially in cases in which a video scanner is used. Using the micrograph partially might result in a modified distribution of the phases present.

5. The increase in scatter with AIA is related to the contrast distribution of the micrograph e.g. between the computer-drawn image A or the electron backscattered image C and the secondary electron images D and E. The phases on micrographs with a wide range of contrast (e.g. the barium titanate micrograph B) are possibly easily recognized by the human eye but are more difficult to distinguish, especially for the automatic method.

6. The determined volume fractions of a microstructure can also be dependent on the exposure conditions used for the micrograph. Whether using an SEM or an optical microscope, decisions have to be made concerning the contrast and brightness, the magnification and the representative area of interest.

7. In order to produce reliable and reproducible results, the determined stereological parameters should converge within the sampled area, which could be in a single or in several micrographs. Depending on the homogeneity of the test sample, this is unlikely to be achieved within a single micrograph. The scatter of volume fraction of zirconia determined by AIA from 77 backscattered electron images of the alumina/zirconia material was considerable. It would clearly be necessary to make measurements on a representative number of micrographs at the magnification used in this round robin before convergence of the average result could be achieved. The individual participants' results within this round-robin in which single micrographs of limited area were employed clearly demonstrate the scatter produced, and indicate the need in practice for several micrographs from each test sample to be analysed to produce reliable mean results.

8. The use of an electron microscope can result in an electrical charge of the non-conductive ceramics during exposure. This can lead to discharges or image distortions, and thin coatings which do not obstruct the contrast differences developed by individual phases should be used. In addition, the topographic effects of sharp edges such as at pores lead to locally enhanced secondary electron image intensity. This can also occur at etched grain boundaries, and it causes a halo in surrounding area. In the alumina/zirconia material, haloes were even seen from sub-surface zirconia grains. This round robin has shown that such features make it much more difficult to differentiate the phases and interpret the images correctly, especially by AIA.

9. In AIA, if the grain or phase boundaries have dark contrast, they may be counted as a separate phase, e.g. if dark they may be indistinguishable from porosity and thus automatically be counted with pores unless the counting process covers only delineated pores. When volume fractions are computed, there is an error, since only the brighter areas of the grains are counted, and the phase boundaries are ignored. Backscattered electron images may thus be more reliably analysed than secondary electron images, and if there is no need to etch or otherwise treat the polished surface in order to visualise the phase contrast, this should not be done.

10. When grain boundaries are counted as a separate dark phase, the true phase volume fractions should be normalised by sharing the grain or phase boundary area in proportion to the volume fractions present. This is a reasonable approximation based on the assumption that the contrast variation is similar on either side of the true

atomically thin boundary. Such a correction is of course inappropriate when the boundary phase is a real phase in its own right and has a finite thickness, e.g. if there is a continuous amorphous phase.

Questions still exist concerning the interpretation of pores and grain pull-outs. However, the preparation of a specimen should be done with care to avoid as far as possible the presence of grain tear-out, and thus avoid the need to make a decision over what is a genuine pore and what is not. It is not entirely clear how each participant has counted the porosity and the bulk material which is visible inside the pores, somewhat underneath the immediate polished surface. The interpretation of the results, for the automatic method, would have been easier if all the digitised and processed images has been returned to the organizers for evaluation.

Furthermore, improved techniques for evaluating the presence of a small amount of phase, for instance pores, along with two or more phases, are worth investigating in the future. The characterisation of such a microstructure would probably need to employ several micrographs with different magnifications scaled to the feature size of the phase of interest.

Acknowledgements

The authors would like to thank sincerely all the participating laboratories for the time and effort expended in undertaking this round robin, and for their contribution in assisting the authors make their conclusions for the directions of standardisation. This work has been supported by the Commission of the European Communities through their mandate for the development of standards placed on CEN TC184/WG3. In addition, support to NPL has been provided by the UK Department of Trade and Industry though the Characterisation of Advanced Materials Programme.

References

[1] L. Dortmans, R. Morrell and G. De With. CEN-VAMAS Round Robin on Grain Size Measurements for advanced Ceramics-Final Report. VAMAS Technical Report 12, 1992. (J.Eur.Ceram.Soc. 12 (3) [1993] 205-13.)

[2] E.R. Weibel, Stereological methods, Vol.1&2, Academic Press inc. (London) Ltd., 1979.

[3] ASTM E1382-91, Determination of average grain size using semiautomatic and automatic image analysis systems.

[4] C. Chatfield, Statistics for technology, 3th edition, 1983, Chapman and Hall, London.

Appendix 1.

Instructions for the Phase Volume Fraction Round Robin

CEN/VAMAS Round Robin on Volume Fraction Measurement

1. Objectives

The round robin is designed to determine the scatter in results that arises from a point-counting method used to determine the volume fraction of phases in multiphase ceramics, and thus to obtain a possible confidence level that can be used in the citation of results. The evaluation also extends to automatic image analysis, providing a comparison between results from different techniques employed in commercial instruments.

2. Options and effort

Participants are welcome to employ either manual image analysis, or automatic image analysis, or both methods, for this work. The total effort required is expected to be no more than 3 person-days for the manual method (no prior experience needed except in preparation of a ceramic sample and taking a micrograph), and 1 additional person-day for the automatic analysis method (some experience with system operation necessary).

Please do not treat this as solely making a measurement. We would very much welcome your comments on the procedure and its wider applicability to ceramic materials. There is space on the "Comments" section on the results sheet, or you can use additional sheets.

3. Materials

3.1 Manual image analysis method:

1 computer-drawn "two phase" micrograph (A)
1 micrograph (B) of a two-phase barium titanate containing some porosity
3 micrographs (C, D, E) of an alumina/zirconia composite ceramic containing some porosity
1 standard transparent 8 mm grid
1 sample of alumina/zirconia ceramic
result sheets

3.2 Automatic image analysis method:

Video/scanner input available:

1 computer-drawn "two phase" micrograph (A)
1 standard transparent 8 mm grid
1 micrograph (B) of a two-phase barium titanate (as for manual method)
3 micrographs (C, D, E) of an alumina/zirconia composite ceramic (as for manual method)
result sheets

or for direct digitised file input:

4 floppy disks with the above images as .TIF files in compressed DOS file format
1 results sheet

4. Procedure

4.1 Manual image analysis method

4.1.1 Objectives

The manual method involves the use of an 8 mm square grid laid over the micrograph. The proportion of grid intersections lying over each phase (including pores) gives the volume fraction of each phase. This requires some interpretation by the operator. Decisions have to be made concerning the position of the grid intersection relative to a feature which may not be clearly defined. Analysis of this round robin will permit the assessment of human perception contributing to the overall uncertainties in the measurement. The series of micrographs supplied (and to be prepared by yourself) will permit some separation of the various factors involved.

4.1.2 Part 1: Supplied micrographs

1. There are five supplied micrographs:
   - A A computer-drawn tessellation, with clear delineation of "grain boundaries" and black/white contrast between the phases.
   - B A secondary electron image of a two-phase barium titanate type ceramic showing a light grey barium titanate phase, a dark grey titanium dioxide phase, and a black phase which is porosity.
   - C A backscattered electron image of an alumina/zirconia ceramic which clearly delineates the zirconia phase (light) and minimises contrast from other features such as thermally etched grain boundaries and shallow pores.
   - D A secondary electron image of the same area as C, but having additional edge contrast from the edges and holes and thermally grooved grain boundaries.
   - E A secondary electron image of a different area from D but with similar contrast from edges and holes (but in this case there is NO accompanying backscattered image!).

2. Place the grid on each of the supplied micrographs (A to E) in turn, and count the grid intersections overlying each phase, including porosity if present, **over the entire area of the image**. (We anticipate that this will give a confidence level of about 2% of the total area). If an intersection, in your opinion, falls exactly on a phase boundary or a pore boundary, count this as 0.5 (in the unlikely but feasible event that the intersection falls precisely on the junction between two phases and a pore, ignore the pore for simplicity!). Micrograph C can be used as an aid to interpretation of Micrograph D.

Note 1: The photos are different sizes, but this should not pose a problem. Do not attempt to count equal numbers of intersections in each image. Micrograph A has no line border. Caution is advised in ensuring a correct count.

3. Place the number of counts for each "phase" on the results form.

4.1.3 Part 2: Own micrograph

1. Mount, grind, polish and if possible, thermally etch the supplied sample of alumina/zirconia composite ceramic, using your normal laboratory techniques.

Note 2: This material may require attention to the polishing procedure to avoid grain tear-out. Ensure that there is adequate removal of prior grinding damage before attempting to polish. The presence of some of grain tear-out may influence the results, and make it more difficult to decide on what is a genuine pore.
Note 3: It is not essential to thermally etch the test-piece, provided that sufficient atomic number contrast is developed by SEM in either secondary electron or backscattered mode to obtain a clear image of the zirconia phase. If thermal etching is employed, etching conditions should be just sufficient to delineate boundaries, but not to create wide regions of contrast or migration of surface material. A nominal temperature of 1450 °C/15 min is probably sufficient.

2. Examine the sample in a SEM and take a secondary electron or backscattered electron SEM photograph (micrograph F) at about 5000 x magnification with the sample normal to incident electron beam. It is not necessary to know the exact magnification, since this is a relative method, but it would be helpful if you could check that there is no more than 2% dimensional distortion of the image screen by using a standard square grid if one is available.

Note 4: If you intend also to undertake the automatic image analysis method, we would prefer that the **same image area** is used as for the manual method. Please read section 4.2.3 first.

3. Enlarge the photograph to a similar size as micrographs A to E (in order to keep the number of intersections of the grid to more than 500). Follow the procedure in Part 1 to determine the volume fractions.

4.2 Automatic image analysis method

4.2.1 Objectives

In automatic image analysis, there are normally in-built routines for undertaking volume fraction analysis based on discrimination between grey levels in a digitised image. However, there are seldom any checks that the instrument software is giving consistent answers. There may also be human factors involved in setting the most appropriate grey levels in first place, and identifying any regions which the computer should ignore in interpreting the image. This part of the round robin is intended to examine the robustness of software in commercial systems and its ability to determine accurately the volume fraction from computer-drawn and real micrographs.

4.2.2 Part1: Supplied micrographs
Note: Please do either 4.2.2.1 or 4.2.2.2, not both!!!

4.2.2.1 Video camera/scanner input option

1. Use your normal techniques for inputting, observing and recording digitally the supplied micrographs. Try to cover most of the area of the micrographs.

2. Use your instrument's conventional programming method or methods to obtain the area fraction of the phases, including porosity.

3. Report the results on the results sheet (e.g. image area pixel count, average intercept proportion, etc.) together with information on the method used (e.g. whether human discrimination was used to eliminate any features from a particular count, problems with setting grey levels, etc.)

4. Input an image of the transparent square grid (back by white paper) used for the manual method. Print a copy of the image obtained and send back with the results. This will be used to check on the level of distortion obtained in inputting the image.

4.2.2.2 Input from compressed .TIF files:

1 Images of micrographs A to E are supplied on 3.5 in. DOS format floppy disks:

Disk 1:	Micrograph A, B	A = TESSEL.exe (1883x1883 pixels)
		B = BATI.exe (1024x1024 pixels)
Disk 2:	Micrograph C	C = PICBSE.exe (1024X1024 pixels)
Disk 3:	Micrograph D	D = PICSE.exe (1024x1024 pixels)
Disk 4:	Micrograph E	E = PICSE2.exe (1024x1024 pixels)
		PICSE3.exe (512x512 pixels)
		PICSE4.exe (256x256 pixels)
		PICSE5.exe (678x512 pixels)

They are supplied in executable compressed format, and can be readily decompressed. Copy the files to your image analyzing computer. Then type, e.g., *BATI*. After a few lines of output you will be asked whether you wish to continue. Type *Yes*. The file will then be decompressed automatically to a standard . TIF file, i.e. *BATI.TIF*, in the same directory.

It has proved too complex to scale the formats to precise individual requirements. If your system cannot handle these formats, you will find only a fraction of the area will be interpreted by your system. However, if your system can convert the full area to a new pixel format, please do this and analyse the full area. For Micrograph E, please choose the largest format size your system can accommodate. Otherwise, **please output a copy of the area analysed (paper copy or .TIF file on a floppy, whichever is easier) and send it with your results.**

2. Employ the instrument's conventional programming method or methods as for the video image input to obtain the area fraction of the phases, including porosity.

3. Report the results on the results sheet, together with information on the area used (i.e.

image area pixel count and position of image compared with the supplied micrographs).

4.2.3 Part 2: Own micrograph

1. Prepare the supplied test piece and obtain a suitable image (Micrograph F) as described in 4.1.3 for the manual method. Input this image either directly into your analysis system (via direct interfacing or a .TIF file as in 4.2.2.2) or from a micrograph (as in 4.2.2.1).
Prepare images of the area examined for supply with your results.

Note: It is preferred that the same area is used for both the manual and automatic image analysis methods. If you have to take different micrographs, please mark them "Manual" and "Auto" respectively.

2. Use the same method as for the video camera input images (as in 4.2.2.1) for determining area fractions of phases and porosity.

3. Report the results on the results sheet (e.g. image area pixel count, average intercept, proportion, etc.). together with information on the method used (e.g. whether human discrimination was used to eliminate any features from a particular count, problems with setting grey levels, etc.).

4. Return of results
Please return your results form, together with copies of any micrograph you have taken (either the original or a laser copy) to:

Dr L.J.M.G. Dortmans
Centre for Technical Ceramics
PO Box 595
5600 AN Eindhoven

Fax: +31 40 244 5619
Email: dortmans@tpd.tno.nl

Please return results by 31 December 1996. Many thanks for taking part!!!

CEN/VAMAS Round Robin on Volume Fraction Measurement

Results form

When completed, please return this form with micrographs of analysed areas to:

Dr L.J.M.G. Dortmans
Centre for Technical Ceramics
PO Box 595
5600 AN Eindhoven

Fax: +31 40 244 5619
Email: dortmans@tpd.tno.nl

Please return results by 31 December 1996

Participant details:

Name:

Name operator if different:

Organisation:

Address:

Telephone: Fax:

Manual Image Analysis Method

Part 1: Supplied micrographs

Results:

	No. of intersections counted:
Micrograph A (computer)	Light "phase":
	Dark "phase":
Micrograph B (barium titanate)	Light phase:
	Dark Phase:
	Porosity (holes, black):
Micrograph C (Al2O3/ZrO2) (Backscattered SEM image)	Alumina (matrix, grey phase):
	Zirconia (particles, light phase):
	Porosity (holes, dark):
Micrograph D (Al2O3/ZrO2) (Secondary SEM image)	Alumina (matrix, grey phase):
	Zirconia (particles, light phase):
	Porosity (holes, dark):
Micrograph E (Al2O3/ZrO2) (Secondary SEM image)	Alumina (matrix, grey phase):
	Zirconia (particles, light phase):
	Porosity (holes, dark):

Comments:

Manual Image Analysis Method

Part 2: Own micrograph from supplied sample

Preparation method:

Thermal etching temperature/time:

Microscope used:

Results:

	No. of intersections counted:
Micrograph F (Al2O3/ZrO2)	Alumina (matrix, grey phase):
	Zirconia (particles, light phase):
	Porosity (holes, dark):

Comments:

Automatic Image Analysis Method

Part 1: Supplied micrographs

Machine type:

Image size (horizontal pixel count x vertical pixel count):

Input type:

Video Input: Yes/No **Scanner Input: Yes/No** **.TIF file Input: Yes/No**
Unless the full micrograph area is used, in order to determine what fraction of the area of each micrograph has been observed by the image analyser, we will need to have an output image from the analyser (or a compressed .TIF file on floppy) in order to correlate results.

Results:

	Area fraction determined:
Micrograph A (computer)	Full image area analysed: Yes/No **If 'No', then please return an image of the area examined.** Light "phase": Dark "phase":
Micrograph B (barium titanate)	Full image area analysed: Yes/No **If 'No', then please return an image of the area examined.** Light phase: Dark phase: Porosity (holes, black):
Micrograph C (Al2O3/ZrO2)	Full image area analysed: Yes/No **If 'No', then please return an image of the area examined.** Alumina (matrix, grey phase): Zirconia (particles, light phase): Porosity (holes, black):

Automatic Image Analysis Method

Part 1: Supplied micrographs (continued)

Micrograph D (Al2O3/ZrO2)	Full image area analysed: Yes/No **If 'No', then please return an image of the area examined.** Alumina (matrix, grey phase): Zirconia (particles, light phase): Porosity (holes, black):
Micrograph E (Al2O3/ZrO2)	If a .TIF file was used, which file did you use: • PICSE2.exe (1024x1024 pixels) • PICSE3.exe (512x512 pixels) • PICSE4.exe (256x256 pixels) • PICSE5.exe (678x512 pixels) Full image area analysed: Yes/No **If 'No', then please return an image of the area examined.** Alumina (matrix, grey phase): Zirconia (particles, light phase): Porosity (holes, black):

For video/scanner input, please supply copy of the image of the transparent grid.

Comments:

Automatic Image Analysis Method

Part 2: Own micrograph from supplied sample

Preparation method:

Thermal etching temperature/time:

Microscope used:

Nominal magnification of image:

Was image directly input to automatic image analyser: Yes/No

Was image input a .TIF file: Yes/No

Was image input via video camera: Yes/No or scanner: Yes/No

Image size (horizontal pixels x vertical pixels):

Results:

	Area fraction determined:
Micrograph F (Al2O3/ZrO2)	Full image area analysed: Yes/No **If 'No', then please return an image of the area examined.**
	Alumina (matrix, grey phase):
	Zirconia (particles, light phase):
	Porosity (holes, black):

Please supply a copy of this image!

Sec next page for comments.

Automatic Image Analysis

Please describe how you think your machine undertakes the measurements, including the names of the software routines employed and steps that you have had to take as an operator to achieve your result.

Other comments on the automatic image analysis applied to these types of samples, including any difficulties encountered.

Appendix 2.

Measurement conditions of the individual participants

Part 1: Supplied Micrographs						
number	**participant number**	**manual method**	**automatic method**	**input method**	**image size**	**total area**
1	1	YES	YES	TIF	MAX	YES
2	2	YES	YES	TIF	512x512	YES
3	3	YES	YES	TIF	512x512	YES
4	4	YES	YES	TIF	256x256 (?)	YES
5	5	YES	YES	TIF/ SCANNER	MAX/ 256x256	YES
6	6	YES	NO			
7	7	YES	YES	TIF	MAX	YES
8	8	YES	YES	TIF	1024x800	YES
9	9	YES	YES	TIF	1024x768	YES
10	10	YES	YES	VIDEO	1024x1024	YES
11	12	YES	YES	TIF	MAX	YES
12	14	YES	YES	TIF	512x512	YES/NO
13	16	YES	YES	TIF	MAX	YES
14	17	YES	NO			
15	18	YES	YES	TIF	MAX	YES
16	19	YES	NO			
17	20	YES	NO			
18	21	YES	YES	TIF	MAX	YES
19	22	YES	YES	TIF	1024x768	NO
21	24	YES	YES	RAS	1024x1024	NO
21	26	YES	NO			
22	28	YES	YES	TIF	MAX	YES
23	29	YES	YES	TIF/ KONTRON	MAX	YES
24	33	YES	YES	TIF	MAX	YES
25	35	YES	YES	TIF	1024x1024	YES
26	36	YES	YES	SCANNER	???	NO
27	37	NO	YES	TIF	MAX/ 1024x1024	YES

Part 2: Supplied Sample/Own Micrograph					
number	**participant number**	**manual method**	**automatic method**	**input method**	**image size**
1	1	NO	NO		
2	2	YES	YES	TIF/ SCANNER	512x512
3	3	YES	YES	TIF	512x512
4	4	YES	YES	SCANNER	636x494
5	5	NO	YES	TIF	256x256
6	6	YES	NO		
7	7	NO	NO		
8	8	YES	YES	TIF/ SCANNER	1860x1400
9	9	YES	YES	TIF	1024x768
10	10	YES	YES	VIDEO	1024x1024
11	12	YES	YES	TIF	1024x1024
12	14	YES	YES	VIDEO	512x512
13	16	YES	NO		
14	17	YES	NO		
15	18	YES	YES	TIF	1024x1024
16	19	YES	NO		
17	20	YES	NO		
18	21	NO	NO		
19	22	YES	YES	TIF	1024x768
21	24	YES	YES	RAS	1024x1024
21	26	YES	NO		
22	28	YES	YES	BMP	1600x1200
23	29	YES	YES		1024x1024
24	33	NO	NO		
25	35	YES	YES		1024x832
26	36	NO	NO		
27	37	NO	NO		

Appendix 3.

Results of the individual participants

Micrographs A and B, Manual image analysis

Number	Participant	Micrograph A				Micrograph B					
		No. intercepts	No. intercepts	Percentage	Percentage	No. intercepts	No.intercepts	No. intercepts	Percentage	Percentage	Percentage
		Light phase	Dark phase	Light phase	Dark phase	Light phase	Dark phase	Porosity	Light phase	Dark phase	Porosity
1	1	293	283	50.87	49.13	333	240.5	2.5	57.81	41.75	0.43
2	2	262	290	47.46	52.54	336.5	237.5	2	58.42	41.23	0.35
3	3	270	259	51.04	48.96	329	197	3	62.19	37.24	0.57
4	4	275.5	292.5	48.50	51.50	345.5	230.5	0	59.98	40.02	0.00
5	5	252.5	276.5	47.73	52.27	342.5	207.5	2	62.05	37.59	0.36
6	6	273	279	49.46	50.54	347	225	4	60.24	39.06	0.69
7	7	268	284	48.55	51.45	313.5	214.5	1	59.26	40.55	0.19
8	8	285.5	293.5	49.31	50.69	333	229	15	57.71	39.69	2.60
9	9	291.5	284.5	50.61	49.39	324.5	249.5	2	56.34	43.32	0.35
10	10	261	291	47.28	52.72	301	222	6	56.90	41.97	1.13
11	12	249.5	279.5	47.16	52.84	334.5	189.5	5.0	63.23	35.82	0.95
12	14	257	272	48.58	51.42	325	223	4	58.88	40.40	0.72
13	16	251.5	277.5	47.54	52.46	332.5	196.5	0	62.85	37.15	0.00
14	17	292.5	283.5	50.78	49.22	339.5	231.5	5	58.94	40.19	0.87
15	18	287	289	49.83	50.17	343	223.5	9.5	59.55	38.80	1.65
16	19	292.5	283.5	50.78	49.22	333	236	7	57.81	40.97	1.22
17	20	259.5	269.5	49.05	50.95	302	214	13	57.09	40.45	2.46
18	21	242	262	48.02	51.98	330	192	1	63.10	36.71	0.19
19	22			46.32	53.68	52.17	38.56	9.27	52.17	38.56	9.27
20	24	262.5	266.5	49.62	50.38	312.5	227.5	0.5	57.82	42.09	0.09
21	26	278	298	48.26	51.74	345.5	228.5	2	59.98	39.67	0.35
22	28	256	259	49.71	50.29	310	229	0	57.51	42.49	0.00
23	29	280	296	48.61	51.39	333	239.5	3.5	57.81	41.58	0.61
24	33	250	279	47.26	52.74	325	200	4	61.44	37.81	0.76
25	35	249.5	277	47.39	52.61	343.5	204	6.5	62.00	36.82	1.17
26	36	274	287	48.84	51.16	341	235	3	58.89	40.59	0.52
27	37										

Micrograph A and B, Automatic image analysis

Number	Participant	Micrograph A			Micrograph B		
		Percentage	Percentage	Percentage	Percentage	Percentage	Percentage
		Light phase	Dark phase	Boundaries	Light phase	Dark phase	Porosity
1	1	46.05	45.89	8.06			
2	2	46	54	0	57.9	42.1	0.8
3	3	47.9	52.1	0	53.64	46.1	0.26
4	4	53.9	46.1	0	65.9	34.1	0.03
5	5	47.65	52.35	0	59	41	0
	5	45.89	46.05	8.06			
6	6						
7	7	45.7	46.2	8.1	57	35.1	7.9
8	8	46	46	8	68.2	31.5	0.2
9	9	52.33	47.67	0	55.8	39.52	4.68
10	10	47.56	52.44	0	51.25	48.65	0.1
11	12	49.92	50.08	0	60.45	39.55	0
12	14	49.7	50.3	0	62.9	36.9	0.2
13	16	49.9	50.1	0	49.2	47.2	3
14	17						
15	18	45.89	46.05	8.06	59	37.6	3.4
16	19						
17	20						
18	21	47	51	0	54	45	1
19	22	49.94	50.06	0	50.78	43.39	5.83
20	24	45.78	54.22	0	59.93	39.64	0.43
21	26						
22	28	47.4	52.6	0	67.2	31.8	1
23	29	45.8	46.1	8.1	54.4	45.1	0.5
24	33	49.91	50.09	0	47.42	48.64	4.41
25	35	45.885	46.042	8.073	55.0272	40.6975	4.1705
26	36	43.41	44.86	11.73	64.12	35.73	0.15
27	37	49.8	50.2	0	54.8	43.95	1.25

Micrograph C, D and E, Manual image analysis

Number	Partic-ipant	Micrograph C						Micrograph D						Micrograph E					
		No. intercepts			Percentage			No. intercepts			Percentage			No. intercepts			Percentage		
		A	Z	Pores	A	Z	Pores	A	Z	Pores	A	Z	Pores	A	Z	Pores	A	Z	Pores
1	1	596.5	33.5	8	93.50	5.25	1.25	600	31	7	94.04	4.86	1.10	575.5	47.5	15	90.20	7.45	2.35
2	2	566.5	41.5	8	91.96	6.74	1.30	574	37	5	93.18	6.01	0.81	571	32.5	12.5	92.69	5.28	2.03
3	3	573	35	8	93.02	5.68	1.30	580	26	8	94.46	4.23	1.30	571	37	8	92.69	6.01	1.30
4	4	600.5	38.5	5	93.25	5.98	0.78	616.5	43	13	91.67	6.39	1.93	624	38.5	4.5	93.55	5.77	0.67
5	5	578	36	2	93.83	5.84	0.32	579	35	2	93.99	5.68	0.32	570.5	37.5	8	92.61	6.09	1.30
6	6	584	30	2	94.81	4.87	0.32	589.5	24.5	2	95.70	3.98	0.32	588	25	3	95.45	4.06	0.49
7	7	575.5	31.5	9	93.43	5.11	1.46	581	27	8	94.32	4.38	1.30	561.5	38.5	16	91.15	6.25	2.60
8	8	580.5	26.5	9	94.24	4.30	1.46	582.5	22.5	11	94.56	3.65	1.79	575.5	29.5	11	93.43	4.79	1.79
9	9	578.5	35.5	2	93.91	5.76	0.32	577	29.5	2.5	94.75	4.84	0.41	578	36.5	1.5	93.83	5.93	0.24
10	10	571	33	12	92.69	5.36	1.95	582	27	7	94.48	4.38	1.14	577	35	4	93.67	5.68	0.65
11	12	526.5	35.5	5	92.86	6.29	0.85	538	26	3	94.90	4.59	0.51	518	30.5	18.5	91.36	5.38	3.26
12	14	562	44	10	91.23	7.14	1.62	570	40	6	92.53	6.49	0.97	571	35	10	92.69	5.68	1.62
13	16	570	37	9	92.53	6.01	1.46	572.5	35.5	8	92.94	5.76	1.30	573	35	8	93.02	5.68	1.30
14	17	587.5	28.5	0	95.37	4.63	0.00	580	34	2	94.16	5.52	0.32	579	30	7	93.99	4.87	1.14
15	18	602	28	8	94.36	4.39	1.25	610.5	22.5	5	95.69	3.53	0.78	581.5	42	14.5	91.14	6.58	2.27
16	19	598	35	5	93.73	5.49	0.78	605	35	4	93.94	5.43	0.62	584	43	11	91.54	6.74	1.72
17	20	571.5	39.5	5	92.78	6.41	0.81	570.5	36.5	9	92.61	5.93	1.46	570.5	34.5	11	92.61	5.60	1.79
18	21	577	20	3	96.17	3.33	0.50	571	30	5	94.22	4.95	0.83	560	36	10	92.41	5.94	1.65
19	22	91.19	6.18	2.63	91.19	6.18	2.63	92.45	5.82	1.73	92.45	5.82	1.73	91.64	5.82	2.55	91.63	5.82	2.55
20	24	601	33.5	2	94.42	5.26	0.31	574	38.5	3	93.26	6.26	0.49	574	35	8	93.03	5.67	1.30
21	26	569	42	5	92.37	6.82	0.81	592	39.5	6	92.86	6.20	0.94	568.5	42.5	9	91.69	6.85	1.45
22	28	576.5	39.5	3	93.13	6.38	0.48	600	39	2	93.60	6.08	0.31	573	43	4.5	92.34	6.93	0.73
23	29	567	38.5	10.5	92.05	6.25	1.70	574	32.5	9.5	93.18	5.28	1.54	573.5	31.5	11	93.10	5.11	1.79
24	33	568	41	7	92.21	6.66	1.14	580	33	3	94.16	5.36	0.49	570	42	4	92.53	6.82	0.65
25	35	629.5	30	7.5	94.38	4.50	1.12	618.5	42.5	6	92.73	6.37	0.90	620	39	8	92.95	5.85	1.20
26	36	585	46	7	91.69	7.21	1.10	601	66	3	89.70	9.85	0.45	591	53	5	91.06	8.17	0.77
27	37																		

Micrograph C, D and E, Automatic image analysis

Number	Participant	Micrograph C			Micrograph D			Micrograph E		
		Percentage Alumina	Percentage Zirconia	Percentage Porosity	Percentage Alumina	Percentage Zirconia	Percentage Porosity	Percentage Alumina	Percentage Zirconia	Percentage Porosity
1	1									
2	2	92.4	6.4	1.2	93.3	6	0.8	92.7	5.7	1.6
3	3	95.23	4.23	0.54	91.77	7.93	0.3	94.65	4.79	0.56
4	4	95	4.9	0.1	94.8	4.8	0.4	94.5	5.2	0.3
5	5									
6	6									
7	7	92.7	4.05	3.25	94.5	5	0.5	90.6	7.6	1.8
8	8	94.7	4.2	1	94.2	5.6	0.2	93.1	6.1	0.8
9	9	94.37	5.07	0.55	94.25	4.51	1.24	93.68	5.26	1.06
10	10	91.18	6.21	2.61	91.98	6.05	1.97	91.5	7.35	1.15
11	12	93.56	5.61	0.82	95.01	4.6	0.39	93.39	5.08	1.53
12	14	94.3	5	0.7	95.3	3.1	1.6	93.3	5.2	1.5
13	16	95.2	4.4	0.3	92.8	6.9	0.3	89.3	9.9	0.3
14	17									
15	18	94.86	4.46	0.73	91.68	7.99	0.33	94.52	4.99	0.49
16	19									
17	20									
18	21	95	4	1	93	5	1	90	6	2
19	22	91.95	6.72	1.33	94.5	3.98	1.52	92.97	5.35	1.68
20	24	94.13	4.39	1.48	92.21	7.09	0.7	85.34	10.35	4.31
21	26									
22	28	93.2	5.6	1.2	92.5	6.5	1	89.3	9.6	1.1
23	29	94.9	4.5	0.6	96	3.6	0.4	94.5	5	0.5
24	33	95.03	4.2	0.57	87.93	10.66	0.39	90.36	8.31	0.42
25	35	94.235	4.82753	1.068	89.794	9.65	0.5543	88.133	9.671	0.61
26	36	94.64	4.94	0.42	93.31	6.45	0.24	86.95	12.68	0.37
27	37	93.52	4.83	1.65	94.3	4.2	1.5	90.77	6.95	2.28

Part 2 Supplied sample, Manual and Automatic image analysis

Number	Participant	Supplied sample, manual			Supplied sample, manual			Supplied sample, automatic		
		No intercepts	No intercepts	No intercepts	Percentage	Percentage	Percentage	Percentage	Percentage	Percentage
		Alumina	Zirconia	Porosity	Alumina	Zirconia	Porosity	Alumina	Zirconia	Porosity
1	1									
2	2	546	78.5	13.5	85.58	12.30	2.12	86.8	11.2	2
3	3	428	38	18	88.43	7.85	3.72	93.71	4.03	2.26
4	4	463	65	0	87.69	12.31	0	91.4	8.6	0
5	5							95	5	0
6	6	665	36	12	93.27	5.05	1.68			
7	7									
8	8	594	48	9	91.24	7.37	1.38	91.7	6.7	1.1
9	9	670	38	5	93.97	5.33	0.70	93.78	5.1	1.12
10	10	582	46	10	91.22	7.21	1.57	89.16	8.97	1.87
11	12	502	39	5	91.94	7.14	0.92	91.77	7.14	1.06
12	14	586	47	5	91.85	7.37	0.78	93.7	6.1	0.2
13	16	568.5	59	10.5	89.11	9.25	1.65			
14	17	86	10	0	89.58	10.42	0			
15	18	513	35	4	92.93	6.34	0.72	94.04	5.65	0.31
16	19	551	59	6	89.45	9.58	0.97			
17	20	571.5	41.5	3	92.78	6.74	0.49			
18	21									
19	22	89.1	9.27	1.63	89.1	9.27	1.63	93.49	5.5	1.01
20	24	325.5	20	6.5	92.47	5.68	1.85	91.93	6.46	1.61
21	26	759	55	2	93.01	6.74	0.25			
22	28	243.5	22.5	18	85.74	7.92	6.34	81.8	9.4	8.8
23	29	496	31	1	93.94	5.87	0.19	94.1	5	0.1
24	33									
25	35	647	75.5	21.5	86.96	10.15	2.89	82.49	13.95	3.51
26	36									
27	37									